Defence Research and Development Canada
Recherche et développement pour la défense Canada

The determination of constant range-difference curves on a spherical surface and its application to emitter geolocation

Stephen H. Sung and Jim P. Y. Lee

Canada

Defence R&D Canada – Ottawa

Technical Memorandum
DRDC Ottawa TM 2009-119
August 2009

The determination of constant range-difference curves on a spherical surface and its application to emitter geolocation

Stephen H. Sung
nEW Technologies Inc.

Jim P. Y. Lee
Defence R&D Canada - Ottawa

Defence R&D Canada – Ottawa

Technical Memorandum
DRDC Ottawa TM 2009-119
August 2009

Principal Author

Original signed by Jim P.Y. Lee

Jim P. Y. Lee

Group Leader/Radar Electronic Warfare Section

Approved by

Original signed by J.F. Rivest

Jean-Francois Rivest

Head/Radar Electronic Warfare Section

Approved for release by

Original signed by Brian Eatock

Brian Eatock

Document Review Panel Chair, DRDC Ottawa

Abstract

This report focuses on the problem of emitter geolocation by measuring the range differences of the emitter from a number of receivers. Two receiver arrangements are considered. In the first arrangement, receiver pairs are located on geographically dispersed platforms. An algorithm is developed that traces out, on essentially the Earth's surface, a curve where each point is at a specified range difference from two receivers. The intersections of such curves, one from the receiver pair on each platform, then yield an estimate of the emitter position. Monte Carlo simulations are carried out to determine the root-mean-square error associated with the intersection point of two such curves. In the second arrangement, several receivers are clustered into an array located on a single platform. Two location estimation methods are employed in Monte Carlo simulations to study the estimation accuracy. In view of the much higher range measurement accuracy required when geolocation is to be performed by a single array, the restriction on the receiver spacing due to space limitations on the platform, and the restriction on the number of receivers due to cost considerations, the first receiver arrangement seems to be the more practical at present.

Résumé

Le présent rapport porte sur la géolocalisation d'émetteurs au moyen des différences entre les distances de l'émetteur par rapport aux divers récepteurs. Deux configurations de récepteurs sont examinées. Pour la première configuration, des paires de récepteurs ont été placées sur des plates-formes géographiquement dispersées. Un algorithme a été mis au point pour dessiner, essentiellement à la surface de la Terre, une courbe dont chaque point correspond à une différence de distance connue de deux récepteurs. Le point d'intersection de ces courbes, une courbe pour la paire de récepteurs de chaque plate-forme, donne la position estimée de l'émetteur. Des simulations de Monte Carlo ont été effectuées afin de déterminer l'erreur quadratique moyenne liée au point d'intersection de ces deux courbes. Pour la seconde configuration, plusieurs récepteurs ont été groupés dans un réseau situé sur une seule plate-forme. Deux méthodes d'estimation de la position sont utilisées dans les simulations de Monte Carlo afin d'étudier la précision des estimations. Étant donné que les mesures de distance utilisées pour effectuer la géolocalisation à partir d'un seul réseau doivent être très précises, que la distance entre les émetteurs est limitée par l'espace disponible sur la plate-forme et que le nombre de récepteurs est limité pour des raisons de coût, la première configuration de récepteurs semble la plus pratique pour le moment.

This page intentionally left blank.

Executive summary

The determination of constant range-difference curves on a spherical surface and its application to emitter geolocation

Stephen H. Sung; Jim P. Y. Lee

DRDC Ottawa TM 2009-119; Defence R&D Canada – Ottawa; August 2009.

Introduction or background: Electronic support measures are integral part of the modern day electronic warfare. The electromagnetic spectrum has to be constantly monitored and analyzed in order to identify any potential threats. One of the key functions that an ESM system performs is passive geolocation of radar emitters. This report focuses on the problem of emitter geolocation by measuring the range differences of the emitter from a number of receivers. Two receiver arrangements are considered. In the first arrangement, receiver pairs are located on geographically dispersed platforms. An algorithm is developed that traces out, on essentially the Earth's surface, a curve where each point is at a specified range difference from two receivers. The intersections of such curves, one from the receiver pair on each platform, then yield an estimate of the emitter position. In the second arrangement, several receivers are clustered into an array located on a single platform. Two location estimation methods are employed in Monte Carlo simulations to study the estimation accuracy.

Results: The correctness of the generated constant range-difference curve is verified in two ways: (1) that each point on the curve is at a range from the Earth centre equal to the radius of the spherical surface, and (2) that the range difference of each point on the curve from the two receivers is indeed the specified value. Monte Carlo simulations are carried out to determine the root-mean-square error associated with the intersection point of two such curves. A two-dimensional location estimator based on triangulation by two stations is considered as a simple model for estimation based on the intersection of two constant range-difference curves. Analytic expressions for the estimated position and the associated root-mean-square error are derived. For the limited number of receiver-pair and emitter arrangements studied, the model seems to give lower bounds on the root-mean-square error. In the case of a single receiver array, two estimation methods, closed-form solution and linearized maximum likelihood, are employed in Monte Carlo simulations to study the estimation accuracy. The closed-form solution method performs somewhat less well than the linearized maximum likelihood method, but has the advantage that an initial estimate of the emitter position is not required. However, both methods perform much less well than the constant range-difference curve intersection method.

Significance: In view of the much higher range measurement accuracy required when geolocation is to be performed by a single array, the restriction on the receiver spacing due to space limitations on the platform, and the restriction on the number of receivers due to cost considerations, the first receiver arrangement seems to be the more practical at present.

Future plans: It may be worthwhile to compare the estimation accuracy from the intersection of two constant range-difference curves with that from the two-dimensional model for additional receiver-pair and emitter arrangements. It may also be useful to compare model predictions with field trial results.

Sommaire

The determination of constant range-difference curves on a spherical surface and its application to emitter geolocation

Stephen H. Sung; Jim P. Y. Lee

DRDC Ottawa TM 2009-119; R & D pour la défense Canada – Ottawa; Août 2009.

Introduction ou contexte: Les mesures de soutien électronique (MSE) font partie intégrante de la guerre électronique moderne. Le spectre électromagnétique doit être constamment surveillé et analysé afin de détecter les menaces éventuelles. L'une des fonctions clés du système MSE est la géolocalisation passive d'émetteurs radar. Le présent rapport porte sur la géolocalisation d'émetteurs au moyen des différences entre les distances de l'émetteur par rapport aux divers récepteurs. Deux configurations de récepteurs sont examinées. Pour la première configuration, des paires de récepteurs ont été placées sur des plates-formes géographiquement dispersées. Un algorithme a été mis au point pour dessiner, essentiellement à la surface de la Terre, une courbe dont chaque point correspond à une différence de distance connue de deux récepteurs. Le point d'intersection de ces courbes, une courbe pour la paire de récepteurs de chaque plate-forme, donne la position estimée de l'émetteur. Pour la seconde configuration, plusieurs récepteurs ont été groupés dans un réseau situé sur une seule plate-forme. Deux méthodes d'estimation de la position sont utilisées dans les simulations de Monte Carlo afin d'étudier la précision des estimations.

Résultats: L'exactitude de la courbe de différence de distance constante produite est vérifiée de deux façons : 1) chaque point sur la courbe est situé à une distance du centre de la Terre qui est égale au rayon de la surface sphérique; 2) la différence de distance pour chaque point sur la courbe représentant les deux récepteurs correspond vraiment à la valeur précisée. Des simulations de Monte Carlo ont été effectuées afin de déterminer l'erreur quadratique moyenne liée au point d'intersection de ces deux courbes. Un estimateur de position en deux dimensions axé sur la triangulation par deux stations est considéré comme étant un modèle simple d'estimation reposant sur l'intersection de deux courbes de différence de distance constante. Des expressions analytiques de la position estimée et de l'erreur quadratique moyenne connexe sont dérivées. Pour les configurations étudiées comportant un nombre restreint d'émetteurs et de paires de récepteurs, le modèle semble imposer des limites inférieures à l'erreur quadratique moyenne. Dans le cas où il y a un seul réseau de récepteur, deux méthodes d'estimation (solution analytique et probabilité maximale linéarisée) sont utilisées dans les simulations de Monte Carlo afin d'étudier la précision des estimations. La méthode de la solution analytique fonctionne un peu moins bien que celle de la probabilité maximale linéarisée, mais elle ne nécessite pas d'estimation initiale de la position de l'émetteur. Les deux méthodes fonctionnent toutefois beaucoup moins bien que la méthode d'intersection des courbes de différence de distance constante.

Importance: Étant donné que les mesures de distance utilisées pour effectuer la géolocalisation à partir d'un seul réseau doivent être très précises, que la distance entre les émetteurs est limitée par l'espace disponible sur la plate-forme et que le nombre de récepteurs est limité pour des raisons de coût, la première configuration de récepteurs semble la plus pratique pour le moment.

Perspectives: Il pourrait être utile de comparer la précision des estimations obtenues par l'intersection de deux courbes de différence de distance constante à la précision des estimations obtenues par le modèle en deux dimensions pour d'autres configurations d'émetteurs et de paires de récepteurs. Il pourrait également être utile de comparer les prédictions des modèles aux résultats obtenus dans le cadre d'essais en conditions réelles.

This page intentionally left blank.

Table of contents

List of figures

List of tables

1 Introduction

The ability to detect, locate and track the movement of ships in Canada's coastal waters is essential to its sovereignty. In this report, we focus on the problem of emitter geolocation based on the time difference of arrival of the emitted signal at a number of receivers, or, equivalently, based on the emitter's range differences (RDs) from the receivers. We consider two receiver arrangements. In the first arrangement, receiver pairs are located on geographically dispersed platforms. In two dimensions, it is well known that an emitter at a fixed RD from two receivers lies on a hyperbola, and therefore the point of intersection of two such hyperbolas gives an estimate of the emitter's position. We generalize this situation to three dimensions, taking the Earth's curvature into account. In Section 2, we describe our algorithm for tracing out, on essentially the Earth's surface, a curve each point of which is at a specified RD from a pair of arbitrarily-oriented receivers. An example of some of the curves generated by our method is then presented. It is pointed out that for an RD that is a substantial fraction of the receiver-pair separation, greater than 90% for example, a constant RD curve may not exist or may exist only partially. The physical reason for this and the associated mathematical manifestation are discussed.

In Section 3, we consider the intersection of two constant RD curves as a way of geolocating a shipborne emitter, which is assumed to be constrained at a certain height above the Earth's surface. Since the emitter and the receiver pairs, if they are moving at all, move over distances that are small compared with the emitter position error that can be tolerated during the time taken for an RD measurement, both the emitter and the receiver pairs are assumed to be stationary in this report. The determination of the point of intersection is described. Monte Carlo simulation results on the accuracy of our method for various arrangements of receiver pairs and emitter are then presented. This method is essentially geolocation based on bearing information, since the measurement of RD at a receiver pair yields the bearing of the hyperbola asymptote. This prompted the consideration, in two dimensions, of geolocation based on triangulation from two receiver pairs with a known separation between them. Analytic expressions for the location estimate and its covariance matrix are derived. The expression for the root-mean-square (RMS) error, which is used as a single quantifier of estimation performance, is expressed in terms of the separation between receiver pairs, the baseline of the receivers of each pair, the range measurement accuracy, and the emitter position. This allows the direct comparison of the RMS error from our simulations with that from the model. Contours of constant RMS error are also generated from the model to show the effect of emitter position on estimation accuracy. They show how the receiver pairs should be oriented relative to the emitter for optimum estimation performance.

In the second receiver arrangement, an array of several receivers is located on a single platform. Here, the emitter position is estimated using a method based on the work of Smith and Abel [1] and Chan and Ho [2]. Reference [3] is an earlier work that discusses emitter geolocation based on RDs, and also addresses the question of emitter position ambiguity. It is possible to obtain a closed-form expression for the emitter position in terms of the set of receiver positions, the set of measured RDs, and the set of range measurement error variances. The derivation of this expression is given in Section 4. Monte Carlo simulation results for various combinations of the

number of receivers in the array, the receiver baseline and the emitter location are presented. The estimation accuracy of this method turns out to be disappointing, at least by the current capability of range-measurement accuracy and the number and spacing of receivers that are likely to be deployed. To verify the correctness of these simulation results, the simulations are repeated using an alternate method. This is the expansion of the RDs in Taylor series about an estimate of the emitter position and retaining only terms to first order in the difference between the actual and the estimated positions [4], [5]. Depending on whether the measurement error statistics are assumed to be Gaussian or not, the emitter position is estimated according to a maximum likelihood criterion or a weighted least squares criterion, respectively. We assume Gaussian measurement error statistics and therefore refer to the method as linearized maximum likelihood (LML). Simulation results based on LML estimation confirm those based on the closed-form solution. Contours of constant RMS error for two-dimensional estimation by the LML method are also generated.

This report is concluded with a summary in Section 5.

2 Determination of Constant Range-Difference Curves on a Spherical Surface

The determination of a constant RD curve on a spherical surface involves four coordinate systems and requires the transformation of a position vector from one coordinate system to another. In Section 2.1, the coordinate systems are defined, and the rotation matrices for coordinate transformations are described. In Section 2.2, the rationale of our method and the computations involved are given. Two main functions (in the MATLAB sense) are needed to generate a constant RD curve. In Section 2.3, the pseudocode for these functions and the main program that calls them to carry out Monte Carlo simulation runs are given. An example of the curves generated by our method is then presented. It is noted that for large RD, and therefore large bearing, a constant RD curve may not exist or may exist only partially. The reason for this and the corresponding mathematical manifestation are given.

2.1 Coordinate Systems & Rotation Matrices

Consider two receivers separated by 2*a*. One receiver is considered to be the reference receiver and is labelled 1. Its position is specified by its longitude Φ_1, its latitude Θ_1, and its height above the mean sea level (MSL) h_1. Its distance from the Earth centre, r_1, is therefore $R_E + h_1$, where R_E is the Earth radius. The position of receiver 2 is specified by three rectangular coordinates in an appropriate coordinate system with origin at receiver 1. For a specified RD, the emitter position is ambiguous, since it can be on either side of the receiver-pair axis. It is assumed that this ambiguity is resolved by prior knowledge or the impossibility for the emitter to be on one side of the pair axis. To specify on which side of the pair axis the emitter is located, the line joining the receivers is considered to be a vector, pointing from receiver 1 to receiver 2. A position specifier is assigned the value of $+1$ if the emitter is on the left of the axis vector, and -1 if the emitter is on the right.

The four coordinate systems involved in the problem are: (1) Earth centred (EC), (2) East-North-Up (ENU), (3) receiver-pair (RX), and (4) final (FINAL). Figure 1(a) shows the relation between the EC and ENU coordinate systems. The origin of EC is at the Earth centre, O. The OX-axis passes through the Greenwich meridian, the OZ-axis passes through the North pole, and the OY-axis is such that XYZ forms a right-handed coordinate system. The ENU has its origin at receiver 1, the U-axis points upward, the E-axis eastward and the N-axis northward. To obtain ENU from EC, we first rotate about the OZ-axis in the counterclockwise direction through Φ_1, then about the new OY-axis counterclockwise through $(90° - \Theta_1)$, then about the latest OZ-axis counterclockwise through 90°. (Since a rotation about an axis results in new directions for the other two axes, in order to simplify the description of rotations below, we will avoid the use of expressions such as “the new OY-axis” and “the latest OZ-axis” and will simply say “the OY-axis” and “the OZ-axis”, with the understanding that the rotation is carried out about the latest direction of the axis.) The result of the three rotations is a coordinate system with the same orientation as ENU but with origin at the Earth centre. This system has to be translated upward

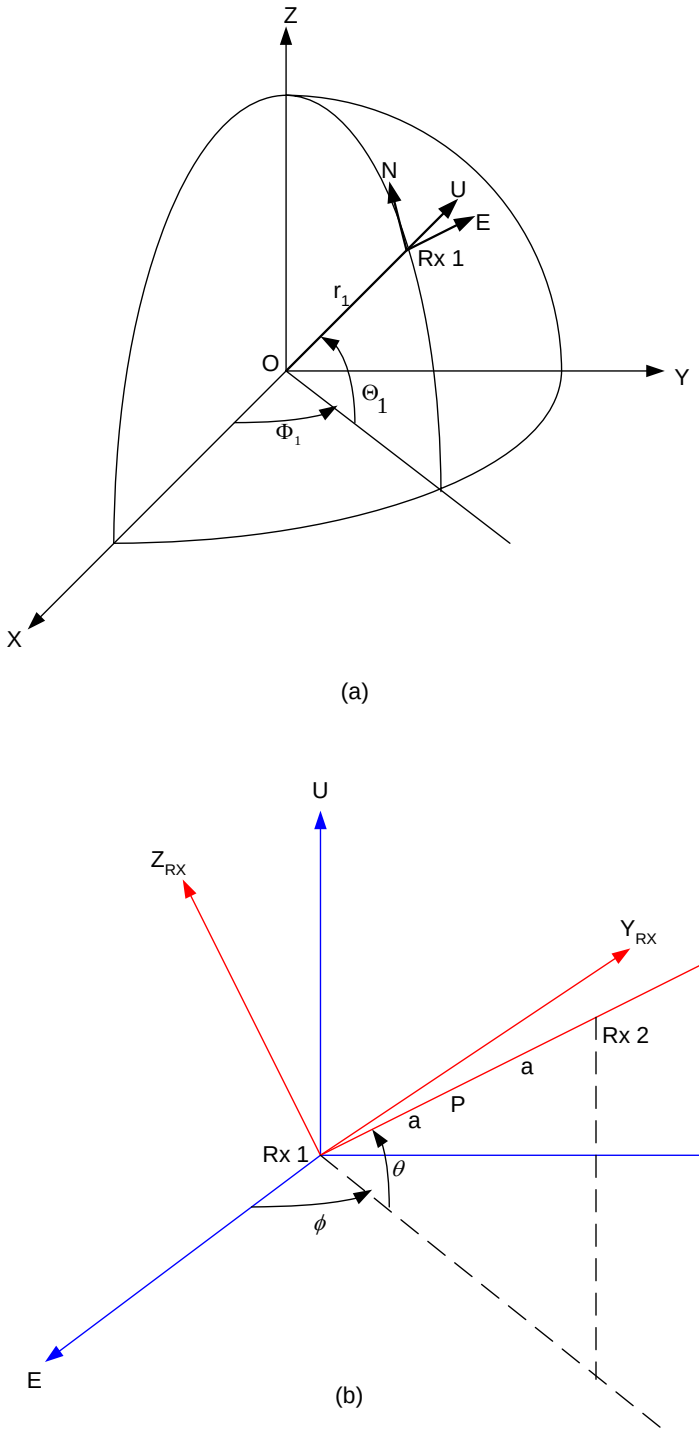

Figure 1: Relations between coordinate systems. (a) EC and ENU; (b) ENU (axes in blue) and RX (axes in red).

by r_1 in order to obtain the ENU with its origin at receiver 1. To avoid confusion, we refer to the ENU with origin at Earth centre as ENUO and that with origin at receiver 1 as simply ENU.

The angle turned through in a rotation is positive for a counterclockwise rotation and negative for a clockwise rotation. The sense of rotation is determined by looking *opposite* to the direction of the rotation axis. The matrices that describe counterclockwise rotations about the *x*-, *y*- and *z*-axis through an angle θ are given by:

$$\mathbf{R}_x(\theta) = \begin{pmatrix} 1 & 0 & 0 \\ 0 & \cos\theta & \sin\theta \\ 0 & -\sin\theta & \cos\theta \end{pmatrix}, \tag{1}$$

$$\mathbf{R}_y(\theta) = \begin{pmatrix} \cos\theta & 0 & -\sin\theta \\ 0 & 1 & 0 \\ \sin\theta & 0 & \cos\theta \end{pmatrix}, \tag{2}$$

$$\mathbf{R}_z(\theta) = \begin{pmatrix} \cos\theta & \sin\theta & 0 \\ -\sin\theta & \cos\theta & 0 \\ 0 & 0 & 1 \end{pmatrix}. \tag{3}$$

Applying these results to the description above for obtaining ENUO from EC, the rotation matrix that transforms a vector in EC to the corresponding vector in ENUO, $\mathbf{R}(\mathrm{EC} \to \mathrm{ENUO})$, is given by:

$$\mathbf{R}(\mathrm{EC} \to \mathrm{ENUO}) = \mathbf{R}_z(\pi/2)\mathbf{R}_y(\pi/2 - \Theta_1)\mathbf{R}_z(\Phi_1). \tag{4}$$

If the position vector of a point in EC is $\mathbf{r}(\mathrm{EC})$, then the position of the same point as observed in ENUO, $\mathbf{r}(\mathrm{ENUO})$, is given by

$$\mathbf{r}(\mathrm{ENUO}) = \mathbf{R}(\mathrm{EC} \to \mathrm{ENUO})\mathbf{r}(\mathrm{EC}). \tag{5}$$

The inverse transformation, from ENUO to EC, is given by

$$\mathbf{r}(\mathrm{EC}) = \mathbf{R}(\mathrm{EC} \to \mathrm{ENUO})^{-1}\mathbf{r}(\mathrm{ENUO}) = \mathbf{R}(\mathrm{EC} \to \mathrm{ENUO})^{\mathrm{T}}\mathbf{r}(\mathrm{ENUO}), \tag{6}$$

where the superscript *T* in the second equality denotes matrix transpose. The second equality follows because a length-preserving rotation matrix is orthogonal and therefore its inverse is equal to its transpose.

Figure 1(b) shows the relation between the ENU and RX coordinate systems. Receiver 2 has azimuth ϕ and elevation θ. The RX coordinate system can be obtained from ENU by first rotating about the U-axis counterclockwise through ϕ, then about the N-axis *clockwise* through

θ. The result is that the two receivers are now along X_{RX}-axis. The rotation matrix for the ENU to RX transformation, $\mathbf{R}(\text{ENU} \rightarrow \text{RX})$, is therefore given by

$$\mathbf{R}(\text{ENU} \rightarrow \text{RX}) = \mathbf{R}_y(-\theta)\mathbf{R}_z(\phi). \tag{7}$$

Figure 2(a) shows the relation between the RX and FINAL coordinate systems. The FINAL coordinate system is obtained by a rotation about the X_{RX} axis *clockwise* through the depression angle δ, so that the RX to FINAL rotation matrix, $\mathbf{R}(\text{RX} \rightarrow \text{FINAL})$, is given by

$$\mathbf{R}(\text{RX} \rightarrow \text{FINAL}) = \mathbf{R}_x(-\delta). \tag{8}$$

2.2 Rationale of Method

In two dimensions, an emitter at a RD, *d*, from two receivers must lie on the hyperbola with the two receivers as foci. For points on a hyperbola far from the origin compared with the foci separation, they are very close to the hyperbolic asymptote, as Figure 3 shows. Since the receiver separation is expected to be of the order of metres, whereas one is interested in locating an emitter which is of the order of kilometres away, one can safely approximate the emitter to be on the asymptote rather than on the hyperbola. Figure 4 shows that the lines joining a distant emitter to two receivers are approximately parallel and that the bearing to the emitter, θ_b, can be determined by measuring the RD *d*, since they are related by

$$\theta_b = \sin^{-1}\left(\frac{d}{2a}\right). \tag{9}$$

The dashed bearing line is, in fact, the asymptote to the hyperbola corresponding to the RD *d*.

Now consider a point on the to-be-determined constant RD curve on the spherical surface. This point must lie in the *xy*-plane of the FINAL coordinate system that has been rotated through an appropriate depression angle δ. Figure 2(b) shows this point on the asymptote, at a distance *s* from the midpoint, P, of the receivers and at a distance *r* from receiver 1. In the FINAL coordinate system, the position of this point is therefore given by

$$\mathbf{r}(\text{FINAL}) = \begin{pmatrix} a + s\cos\alpha \\ s\sin\alpha \\ 0 \end{pmatrix}, \tag{10}$$

where α can be computed from the bearing according to

$$\alpha = sign \times (\pi/2 - \theta_b), \tag{11}$$

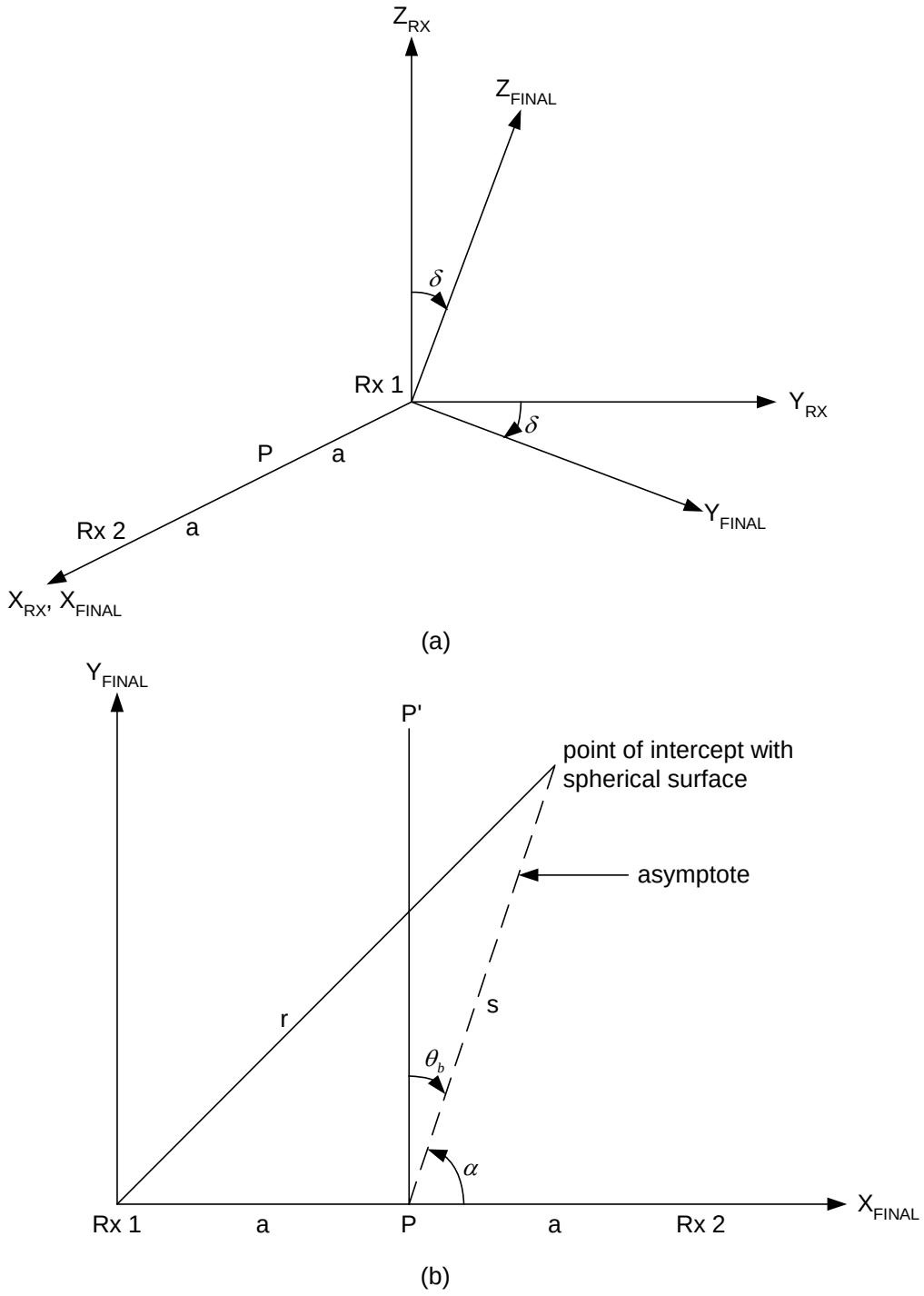

Figure 2: (a) Relation between RX and FINAL coordinate systems; (b) xy*-plane of FINAL coordinate system.*

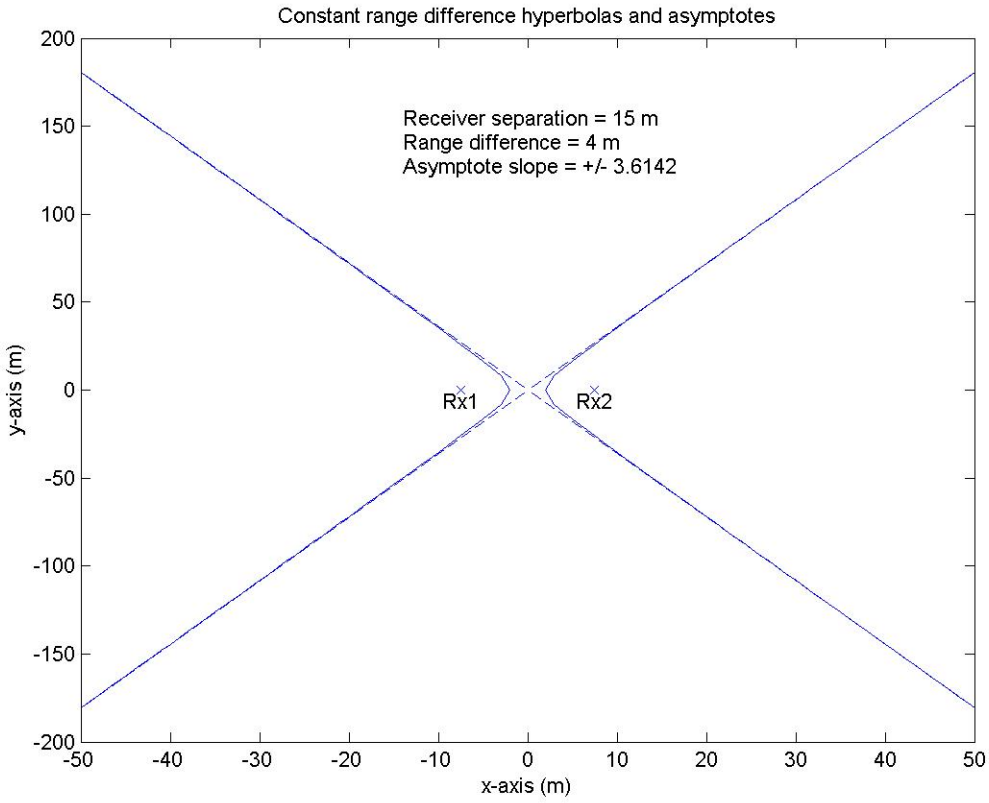

Figure 3: Constant-range-difference hyperbolas and their asymptotes (dashed lines).

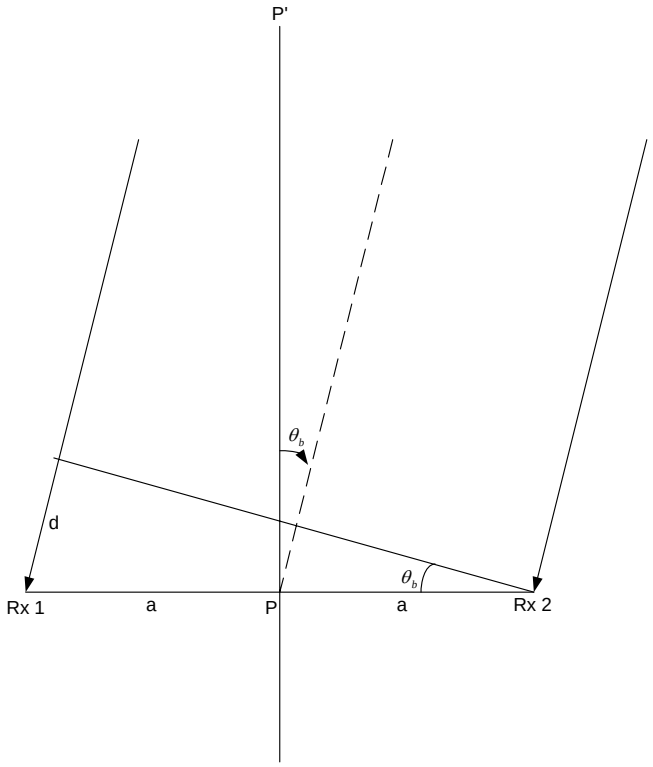

Figure 4: The lines joining two receivers to a distant emitter, showing the relation between the range difference, d, and the bearing, θ_b.

where *sign* is the specifier of on which side of the receiver-pair axis the emitter is located. In Figure 2(b), *sign* is $+1$. It should be mentioned that we use the convention that RD is defined as the range of emitter from receiver 1 minus the range of emitter from receiver 2. The bearing is therefore positive for an emitter to the right of the receiver-pair perpendicular bisector $\mathrm{P}'\mathrm{P}$ and negative to its left.

When viewed in the ENU coordinate system, the intersection point is still at range *r* from receiver 1, since this range is independent of coordinate system. This range corresponds to a particular depression angle, Δ, in ENU, since these two quantities are related. There is azimuthal symmetry about the U-axis, so that the relation between *r* and Δ can be considered in a plane, as shown in Figure 5. What is needed is a relation between δ and Δ, and this can be obtained as follows. From **r**(FINAL) as given by Eq. (10), we transform it to the ENU coordinate system by computing

$$\mathbf{R}(\mathrm{ENU} \rightarrow \mathrm{RX})^T \, \mathbf{R}(\mathrm{RX} \rightarrow \mathrm{FINAL})^T \, \mathbf{r}(\mathrm{FINAL}) \, .$$

Then from the rectangular components of this vector, we can determine Δ. After some algebra, we find that

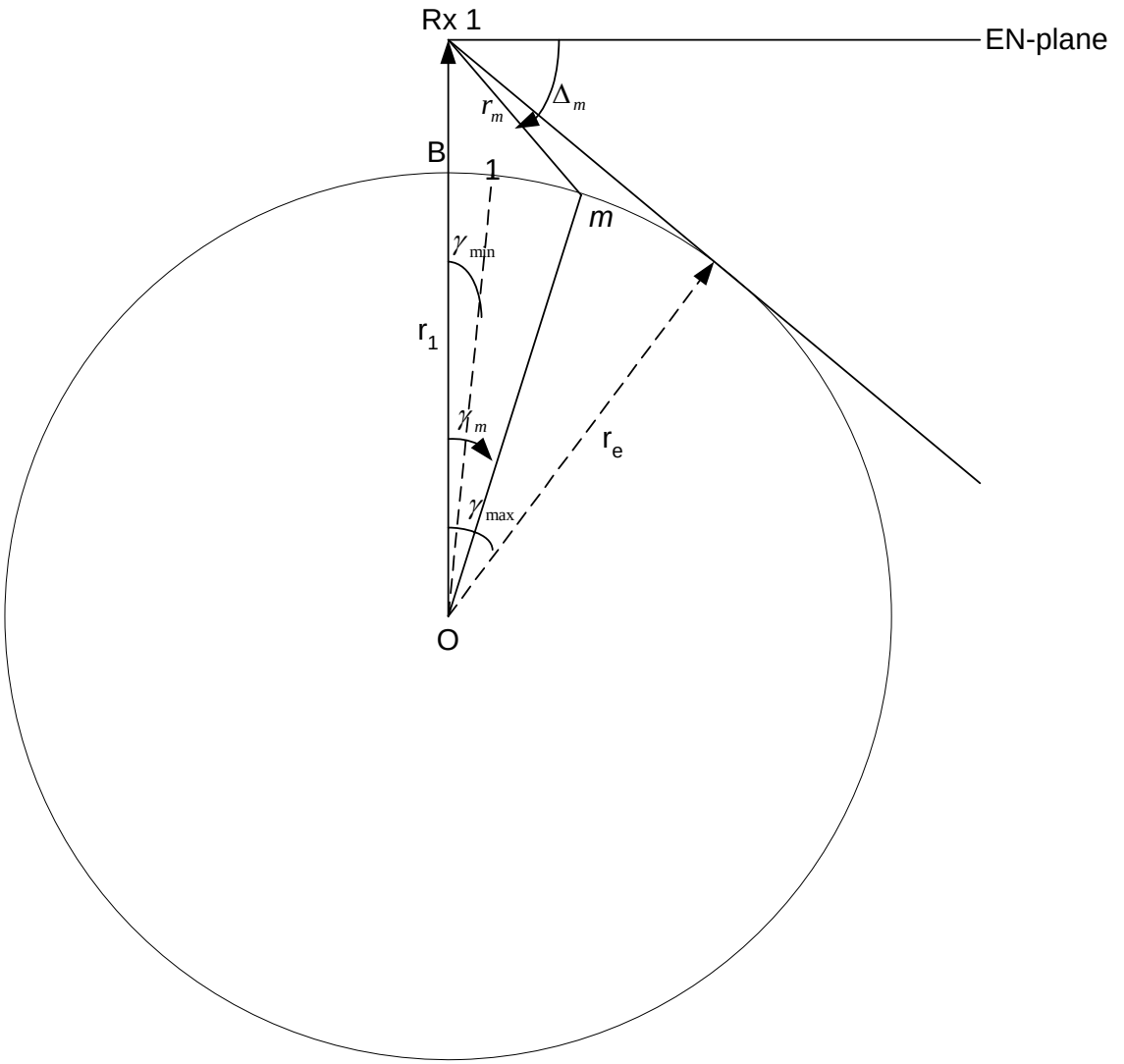

Figure 5: M *equally-spaced points on a circumference passing through receiver 1, showing the angle subtended by the* m*th point,* γ_m*, and the associated slant range* r_m *and depression angle* Δ_m.

$$\sin\delta = \frac{r\sin\Delta + (a + s\cos\alpha)\sin\theta}{s\sin\alpha\cos\theta}. \tag{12}$$

We also need a relation between *s* and *r*. From Figure 2(b),

$$r^2 = (a + s\cos\alpha)^2 + (s\sin\alpha)^2.$$

Expressing *s* in terms of *r*, we obtain the quadratic equation

$$s^2 + (2a\cos\alpha)s - (r^2 - a^2) = 0 .$$

The solution is

$$s = \sqrt{r^2 - a^2 \sin^2 \alpha} - a\cos\alpha , \tag{13}$$

where we have chosen the solution corresponding to the plus sign, since the minus sign gives the physically unreasonable solution of negative *s*.

Our problem can be solved by simply considering a series of *r* values, from some minimum range to some maximum range, such as the distance to the horizon. For each *r*, we compute Δ. Then from Eqs. (12) and (13), we obtain δ and *s*. This means that we know the coordinates of the intercept point in the FINAL coordinate system and by how much the RX coordinate system must be rotated to give the FINAL coordinate system. We can then carry out a series of inverse coordinate transformations: from FINAL to RX to ENU to EC. The rectangular coordinates of the intercept point in EC are then converted to longitude and latitude.

For the series of *r* values, we consider *M* uniformly spaced points on the circumference of the circle in Figure 5. The points extend from a start range r_0, measured along the circumference from point B and specified by the user, to the horizon. A typical value of r_0 may be 2 km. The radius of the circle, r_e, is $R_E + h_e$, where h_e is the assumed height of the emitter above the MSL. The minimum subtended angle, $\gamma_{\min}$, is therefore r_0 / r_e, the maximum, $\gamma_{\max}$, is $\cos^{-1}(r_e / r_1)$. The set of uniformly subtended angles is then given by

$$\gamma_m = \gamma_{\min} + \frac{\gamma_{\max} - \gamma_{\min}}{M}(m-1), \qquad m = 1, \ldots, M . \tag{14}$$

By the cosine law, the slant range, r_m, corresponding to γ_m is given by

$$r_m = \sqrt{r_1^2 + r_e^2 - 2r_1 r_e \cos\gamma_m} , \tag{15}$$

and by the application of the sine law, the corresponding depression angle, Δ_m, is found to be

$$\tan\Delta_m = \frac{r_1 / r_e - \cos\gamma_m}{\sin\gamma_m} . \tag{16}$$

It should be pointed out that the choice of uniformly spaced points on the circumference is simply a way of obtaining a range of *r* values that encompasses all ranges from receiver 1 to points on a constant RD curve. The intercept points on such a curve are, in general, not equally spaced.

For each r_m, Δ_m pair, we compute δ_m and s_m from Eqs. (12) and (13). In the FINAL coordinate system, the position of the *m*th intercept point, $\mathbf{r}_m(\text{FINAL})$, is then given by

$$\mathbf{r}_m(\text{FINAL}) = \begin{pmatrix} a + s_m \cos\alpha \\ s_m \sin\alpha \\ 0 \end{pmatrix}. \tag{17}$$

Inverse transforming to the RX system, we obtain, by the use of Eq. (8),

$$\mathbf{r}_m(\text{RX}) = \mathbf{R}_x(-\delta_m)^T \mathbf{r}_m(\text{FINAL}), \tag{18}$$

and inverse transforming to ENU, we have

$$\mathbf{r}_m(\text{ENU}) = \mathbf{R}(\text{ENU} \to \text{RX})^T \mathbf{r}_m(\text{RX}). \tag{19}$$

In the ENU system, we must add r_1 to the third component of $\mathbf{r}_m(\text{ENU})$ to obtain the intercept vector in the ENUO coordinate system, which is then inverse transformed to the EC system to give

$$\mathbf{r}_m(\text{EC}) = \mathbf{R}(\text{EC} \to \text{ENUO})^T \left[\mathbf{r}_m(\text{ENU}) + \begin{pmatrix} 0 \\ 0 \\ r_1 \end{pmatrix} \right]. \tag{20}$$

The longitude and latitude of the intercept point can then be obtained from $\mathbf{r}_m(\text{EC})$.

2.3 Pseudocode

In this section, we present the pseudocode for the main program, called Main, that carries out the Monte Carlo simulations with results given in Section 3. The two key functions involved in the determination of a constant RD curve are referred to as Function1 and Function2. Function1 calculates the set of slant ranges r_m and depression angles Δ_m, $m = 1, \ldots, M$. Function2 carries out the inverse transformation of intercept vectors from the FINAL to the EC coordinate system, thereby tracing out the required curve. The calculations are divided into two functions because those carried out by Function1 need to be done only once for each receiver pair, whereas those performed by Function2 need to be carried out thousands of times in a Monte Carlo simulation.

Main

The user specifies the following:
(a) Number of receiver pairs;
(b) Spherical coordinates of receiver 1 of each pair;
(c) Rectangular coordinates of receiver 2 of each pair, measured in the ENU system with origin at the associated receiver 1;

(d) *sign* value that specifies on which side of the receiver-pair axis the emitter is located;
(e) Spherical coordinates of emitter;
(f) Range measurement error standard deviation;
(g) Start range of constant RD curve, r_0, and number of points per curve, *M*;
(h) Number of trials in a simulation run;
(i) Constants such as Earth radius and degrees per radian.

The following calculations need to be carried out once or once per receiver pair:
(a) Convert spherical coordinates of receiver 1 of each pair to rectangular coordinates (in the EC system);
(b) Convert spherical coordinates of emitter to rectangular coordinates;
(c) Determine separation between receiver 2 and associated receiver 1, the azimuth ϕ and the elevation θ of receiver 2, for each receiver pair;
(d) Calculate the rotation matrix $\mathbf{R}(\text{EC} \rightarrow \text{ENUO})$, one for each receiver pair;
(e) Make use of $\mathbf{R}(\text{EC} \rightarrow \text{ENUO})$ to calculate the rectangular coordinates of receiver 2 of each pair in the EC system, remembering to add the associated receiver 1's distance from Earth centre to the third component of receiver 2's ENU coordinates before inverse transformation;
(f) Calculate the rotation matrix $\mathbf{R}(\text{ENU} \rightarrow \text{RX})$, one for each receiver pair;
(g) Call Function1 to calculate *M* slant ranges and depression angles, one set for each receiver pair;
(h) Calculate true range of receiver 1 of each pair from emitter;
(i) Calculate true range of receiver 2 of each pair from emitter.

The following processing is carried out inside the simulation loop, once for each trial:

For each receiver pair,

Simulate measured range from emitter to receiver 1 by adding to the true range a Gaussian distributed random number of zero mean and standard deviation equal to the specified measurement error standard deviation;
Simulate measured range from emitter to receiver 2 in the same way;
Subtract second quantity from first to obtain measured RD;
Call Function2 to trace out the constant RD curve.

Find the intersection point of the first two constant RD curves. (At present, the user can specify more than two receiver pairs, but the intersection point is based on the RD curves of only the first two pairs.) The intersection point is an estimate of the latitude and longitude of the emitter, stored in the 2×1 vector $\hat{\mathbf{x}}_e$.

Save $\hat{\mathbf{x}}_e$ in an array with number of columns equal to the number of trials for subsequent plotting.

Accumulate the outer product $\hat{\mathbf{x}}_e \hat{\mathbf{x}}_e{}^T$.

Upon completion of the trials, calculate simulation run statistics, the most important of which are:
(a) the mean estimate;
(b) the estimate covariance matrix;
(c) the bias;
(d) the RMS error, in units of metre rather than radian.

All user-specified values; calculated quantities such as rotation matrices, slant ranges and depression angles; and simulation estimates and statistics are saved to a file.

Function1

Inputs:
(a) Start range of constant RD curve, r_0, and number of points per curve, *M*;
(b) Receiver 1 range from Earth centre, r_1;
(c) Emitter range from Earth centre, r_e.

Outputs:
Slant ranges and depression angles, $r_m, \Delta_m, m = 1, \ldots, M$.

Calculations:
(a) Compute minimum subtended angle $\gamma_{\min}$, maximum subtended angle $\gamma_{\max}$, and equally spaced subtended angles $\gamma_m, m = 1, \ldots, M$;
(b) Calculate r_m according to Eq. (15);
(c) Calculate Δ_m according to Eq. (16).

Function2

Inputs:
(a) Measured RD, *d*;
(b) Separation between receivers 1 and 2, 2*a*;
(c) *sign* value;
(d) Receiver 1 range from Earth centre, r_1;
(e) Receiver 2 elevation angle, θ;
(f) Slant ranges and depression angles, $r_m, \Delta_m, m = 1, \ldots, M$;
(g) Rotation matrix $\mathbf{R}(\text{EC} \rightarrow \text{ENUO})$;
(h) Rotation matrix $\mathbf{R}(\text{ENU} \rightarrow \text{RX})$.

Outputs:
(a) $M \times 1$ array of longitude of intercept points that define the constant RD curve;
(b) $M \times 1$ array of latitude of intercept points that define the constant RD curve.

Calculations:
For each intercept point,
(a) Calculate bearing θ_b according to Eq. (9);
(b) Calculate α according to Eq. (11);
(c) Calculate s_m according to Eq. (13) with *r* equal to r_m;
(d) Calculate δ_m according to Eq. (12) with *r* equal to r_m, Δ equal to Δ_m, and *s* equal to s_m;
(e) Form the vector $\mathbf{r}_m(\text{FINAL})$ according to Eq. (17);

(f) Calculate $\mathbf{r}_m(\mathrm{RX})$ according to Eq. (18);

(g) Calculate $\mathbf{r}_m(\mathrm{ENU})$ according to Eq. (19);

(h) Calculate $\mathbf{r}_m(\mathrm{EC})$ according to Eq. (20);

(i) Calculate longitude and latitude of intercept point from $\mathbf{r}_m(\mathrm{EC})$.

As an application of Function1 and Function2, 15 constant RD curves are generated for RDs that yield bearings from –70° to 70° in steps of 10°. These curves are shown in red in Figure 6. The receivers are separated by 15 m and both are at the same height of 400 m above MSL. At this height, the distance to the horizon is 71.4 km. The start range r_0 is chosen to be 2 km. Therefore, each curve extends from about 2 km to about 71 km and consists of 50 points. The emitter height is 10 m above MSL. Each curve is thus on a spherical surface of radius $r_e = R_E + 10$ m. The curvature of the curves can be clearly seen. The blue lines are the projections of the curves on the EN-plane of the ENU coordinate system. For the 30° bearing curve, the green lines connect five chosen points on the curve with their projections.

That the curves are generated correctly can be readily checked in two ways. First, each point on a curve must be at a range of r_e from the Earth centre. Second, each point on a curve must have a RD from the receivers equal to the specified RD for generating that curve. Each point of each curve is found to satisfy both checks. For the second check, for example, the RD calculated from the distances of a point on a curve from the receivers differs from the specified RD by less than 4×10^{-5} m at the shortest range and less than 10^{-7} m at the longest range.

It should be pointed out that if the bearing is too large, and therefore α too small, there can be no solution to Eq. (12). This is because a constant RD curve is the intersection of a cone, with apex at the midpoint of the two receivers and half angle α, with the spherical surface. If α is too small, there is no intersection at all or there is intersection at long ranges but not at short ranges. Consider the special case where the receivers are at the same height above MSL. Then the receiver 2 elevation angle, θ, is zero, and Eq. (12) reduces to

$$\sin\delta = \frac{r\sin\Delta}{s\sin\alpha}. \tag{21}$$

If α is too small, the right hand side can exceed unity for *r*, Δ, and *s* at some point *m* along the curve, but the left hand side must be less than or equal to unity, and therefore there is no solution for δ at that point.

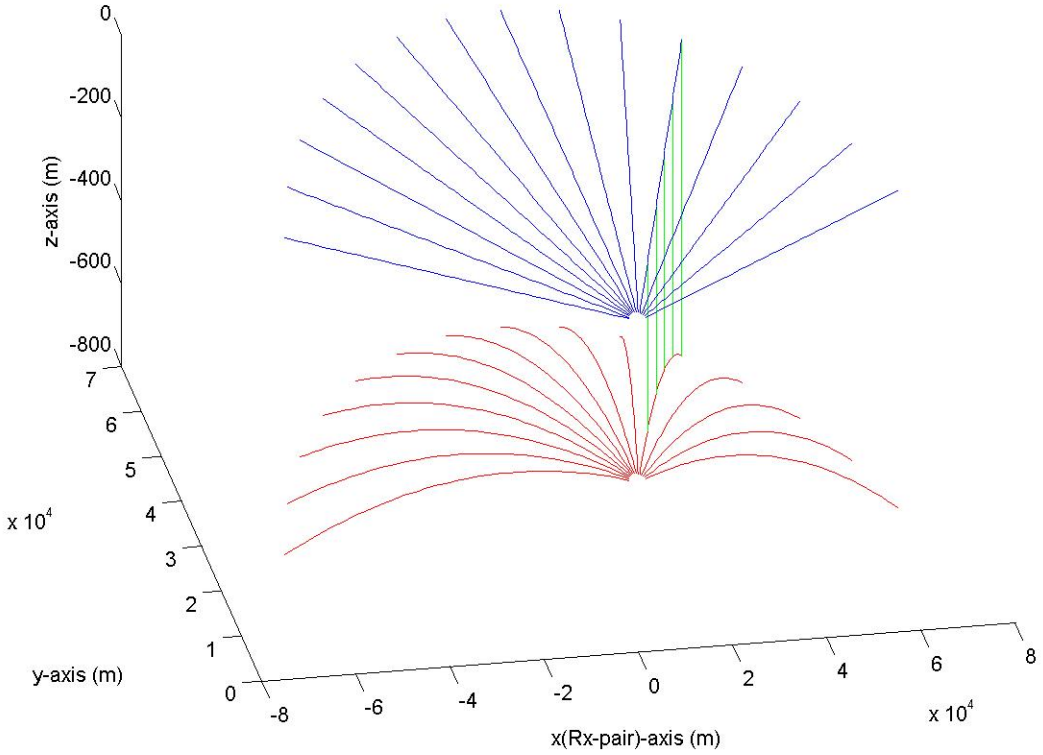

Figure 6: Fifteen constant-range-difference curves on the spherical surface on which the emitter is located (in red), corresponding to bearings from –70° to 70° in steps of 10°, and their projections (in blue) on the horizontal plane passing through the receivers. The green lines link five points on the constant range-difference curve of bearing 30° with their projections. The vector from receiver 1 to receiver 2 points East, the receivers are separated by 15 m and are at the same height of 400 m above MSL. The emitter is at a height of 10 m above MSL.

3 Receiver Pairs on Geographically Dispersed Platforms

The determination of the intersection point of two constant RD curves is given in Section 3.1. Some Monte Carlo simulation results are presented in Section 3.2. The geolocation method of this section is essentially location by bearing. The estimation accuracy of a bearing-based method in two-dimensions is worked out and compared with that from the simulation results.

3.1 Determination of Intersection Point

In the neighbourhood of the intersection point of two constant RD curves, the curves are linear to a very good approximation. Therefore, the intersection point is determined by finding the intersection point of two straight lines. This is shown in Figure 7, where the four circles mark the point just before and the point just after intersection for each of the two curves. Each point is described by the longitude-latitude pair (ϕ, θ). The first subscript, 1 or 2, specifies the curve and the second subscript specifies the position relative to the intersection point: "b" for before and "a" for after the intersection point. The intersection point has coordinates ϕ_0 and θ_0.

The slopes of the two lines, s_1 and s_2, are given by

$$s_1 = \frac{\theta_{1a} - \theta_{1b}}{\phi_{1a} - \phi_{1b}}, \qquad s_2 = \frac{\theta_{2a} - \theta_{2b}}{\phi_{2a} - \phi_{2b}}. \tag{22}$$

The two lines are therefore described by the equations

$$\theta = s_1(\phi - \phi_{1b}) + \theta_{1b}, \qquad \theta = s_2(\phi - \phi_{2b}) + \theta_{2b}. \tag{23}$$

At the intersection point, ϕ_0 and θ_0 must satisfy both equations. The solution is found to be

$$\begin{aligned} \theta_0 &= \frac{s_1 s_2(\phi_{1b} - \phi_{2b}) + s_1\theta_{2b} - s_2\theta_{1b}}{s_1 - s_2}, \\ \phi_0 &= \frac{s_1\phi_{1b} - s_2\phi_{2b} + \theta_{2b} - \theta_{1b}}{s_1 - s_2}. \end{aligned} \tag{24}$$

Numerically, after the two constant RD curves are determined, one computes the longitude difference between the two curves and finds where this difference changes sign. The coordinates of the four points can then be obtained.

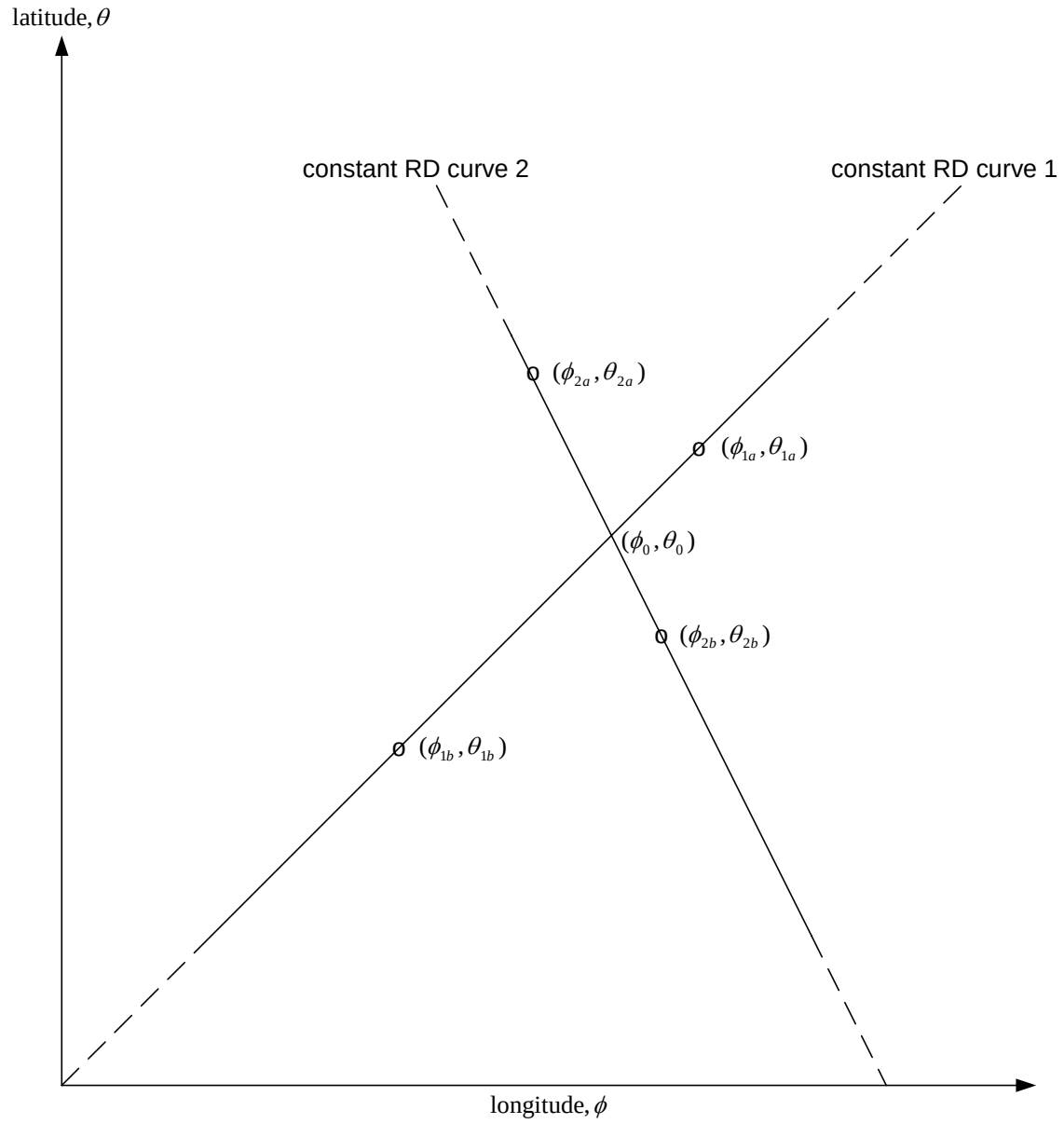

Figure 7: Two constant range-difference curves in the neighbourhood of their intersection point, showing the longitude and latitude of the points just before and just after intersection for each of the two curves.

3.2 Simulation Results

The processing in the simulation main program is described by the pseudocode of Main in Section 2.3. Here, we first comment on the measurement error model. This model is used in this section and in Section 4. The error, ε, is that in the measurement of a *range* rather than a range difference by a receiver. The error in the measurement of a range difference is taken to be

a difference of two ε's. The range measurement error is modelled as a Gaussian random variable of zero mean and variance σ^2:

$$\bar{\varepsilon} = 0, \qquad \overline{\varepsilon^2} = \sigma^2, \tag{25}$$

where the overbar denotes expected value. All receivers are assumed to have the same range measurement error variance.

The estimates from all the trials of a simulation run are processed to obtain the following statistics. For each trial, we obtain a latitude estimate, $\hat{\theta}_e$, and a longitude estimate, $\hat{\phi}_e$, for the emitter. These estimates are stored as elements 1 and 2, respectively, of the vector $\hat{\mathbf{x}}_e$:

$$\hat{\mathbf{x}}_e = \begin{pmatrix} \hat{\theta}_e \\ \hat{\phi}_e \end{pmatrix}. \tag{26}$$

Typically, a simulation run involves 2000 trials. The 2000 estimates are stored for subsequent plotting purposes. Upon averaging over the trials, we obtain the mean estimate:

$$\overline{\hat{\mathbf{x}}_e} = \begin{pmatrix} \overline{\hat{\theta}_e} \\ \overline{\hat{\phi}_e} \end{pmatrix}. \tag{27}$$

The estimate covariance matrix, **C**, is calculated according to

$$\mathbf{C} = \overline{\hat{\mathbf{x}}_e \hat{\mathbf{x}}_e{}^T} - \left(\overline{\hat{\mathbf{x}}_e}\right)\left(\overline{\hat{\mathbf{x}}_e}\right)^T, \tag{28}$$

where the first term is obtained by accumulating $\hat{\mathbf{x}}_e \hat{\mathbf{x}}_e{}^T$ over the trials and then dividing by the number of trials. The bias, **b**, is by definition

$$\mathbf{b} = \overline{\hat{\mathbf{x}}_e} - \mathbf{x}_e, \tag{29}$$

where $\mathbf{x}_e$ contains the true emitter latitude and longitude. We then compute the matrix **E**, defined to be

$$\mathbf{E} = \mathbf{C} + \mathbf{b}\mathbf{b}^T. \tag{30}$$

The diagonal elements of **E**, E_{11} and E_{22}, are the mean square errors of the latitude and longitude estimates, respectively. These elements are in units of radian^2. It gives one a better feel for the estimation performance if the RMS error, ε_r, is expressed in metres rather than in radians. Therefore, we multiply E_{11} by r_e^2 and E_{22} by $r_e^2 \cos^2\left(\overline{\hat{\theta}_e}\right)$, add them and take the square root to obtain

$$\varepsilon_r = r_e \sqrt{E_{11} + \cos^2\left(\overline{\hat{\theta}_e}\right) E_{22}} \ . \tag{31}$$

We use ε_r as a single quantifier of estimation performance.

Figure 8 shows the simulation results for two emitter positions. The two receiver pairs, marked by the "x" plot symbols on the horizontal axis, are separated by 4 km. The receivers of each pair are separated by 10 m. The range measurement error standard deviation, σ, is 0.1 m. The emitter is located halfway between the receiver pairs, at 10 km and 15 km North of the pairs. The first 1000 estimates and the 95% concentration ellipse are shown in blue and magenta, respectively, for the two locations. The RMS errors calculated according to (31) are shown next to the respective clusters. As one would expect, the RMS error increases as the emitter range increases.

Figure 9 shows the results for two receiver pair separations, 4 km for the pairs marked by "x" and 6 km for the pairs marked by "o". The emitter is 15 km North of the pairs. The first 1000 estimates and the 95% concentration ellipse are shown in blue and magenta, respectively, for the 4 km and 6 km separations. The smaller RMS error is for the magenta cluster, indicating better estimation performance as the pair separation increases.

3.3 Two-Dimensional Geolocation by Bearing Measurements

Figure 10 shows the determination of an emitter's position based on the bearings θ_1 and θ_2 measured by two stations separated by a known distance 2*l*. The emitter coordinates *x*, *y* are with respect to the coordinate system origin O. In terms of θ_1, θ_2 and *l*, the emitter coordinates are given by

$$x = \frac{l \sin(\theta_1 + \theta_2)}{\sin(\theta_1 - \theta_2)}, \qquad y = \frac{2l \cos\theta_1 \cos\theta_2}{\sin(\theta_1 - \theta_2)}. \tag{32}$$

The errors in *x* and *y*, δx and δy, due to errors in the bearings, $\delta\theta_1$ and $\delta\theta_2$, can be determined from

$$\delta x = \left(\frac{\partial x}{\partial \theta_1}\right)\delta\theta_1 + \left(\frac{\partial x}{\partial \theta_2}\right)\delta\theta_2, \qquad \delta y = \left(\frac{\partial y}{\partial \theta_1}\right)\delta\theta_1 + \left(\frac{\partial y}{\partial \theta_2}\right)\delta\theta_2. \tag{33}$$

In our case, each station is a pair of receivers where the bearing is determined from the RD according to Eq. (9). Therefore,

$$\delta\theta_1 = \frac{\varepsilon_1 - \varepsilon_2}{2a\cos\theta_1}, \qquad \delta\theta_2 = \frac{\varepsilon_3 - \varepsilon_4}{2a\cos\theta_2}, \tag{34}$$

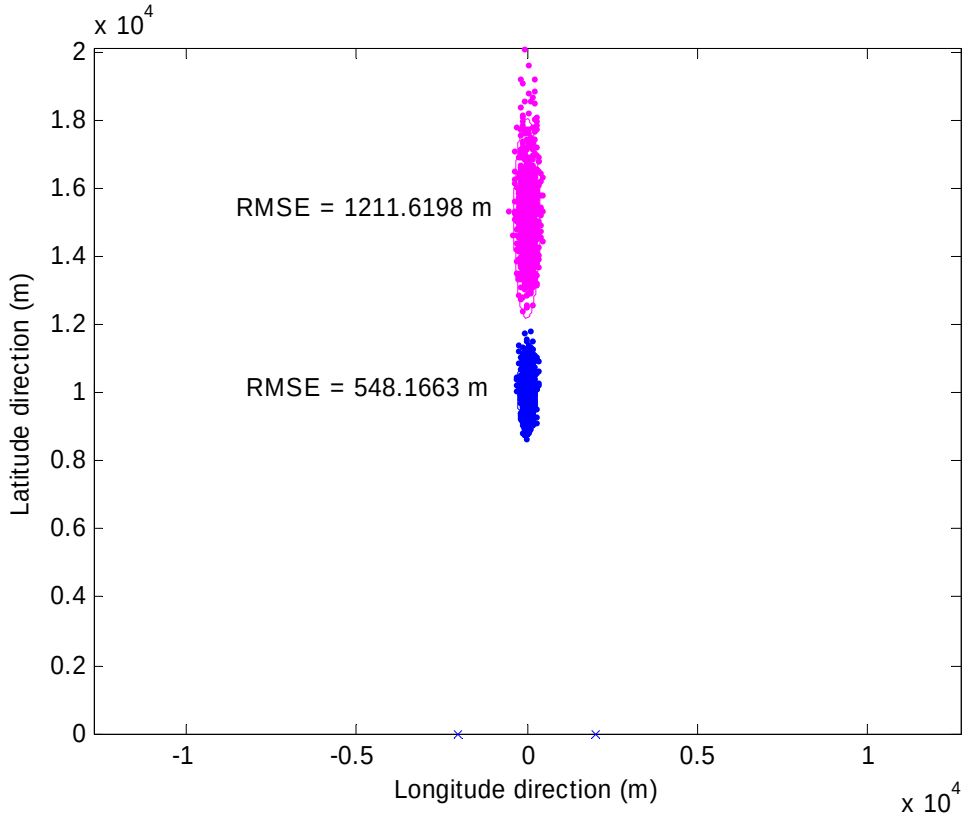

Figure 8: Comparison of location estimates for two emitter positions along the perpendicular bisector of the line joining two receiver pairs. The "x" plot symbols mark the two receiver pairs separated by 4 km. The blue dots and ellipse show the 1000 estimates and the 95% concentration ellipse for an emitter at 10 km from the midpoint of the line joining the two receiver pairs. The corresponding estimates for an emitter at 15 km are shown in magenta.

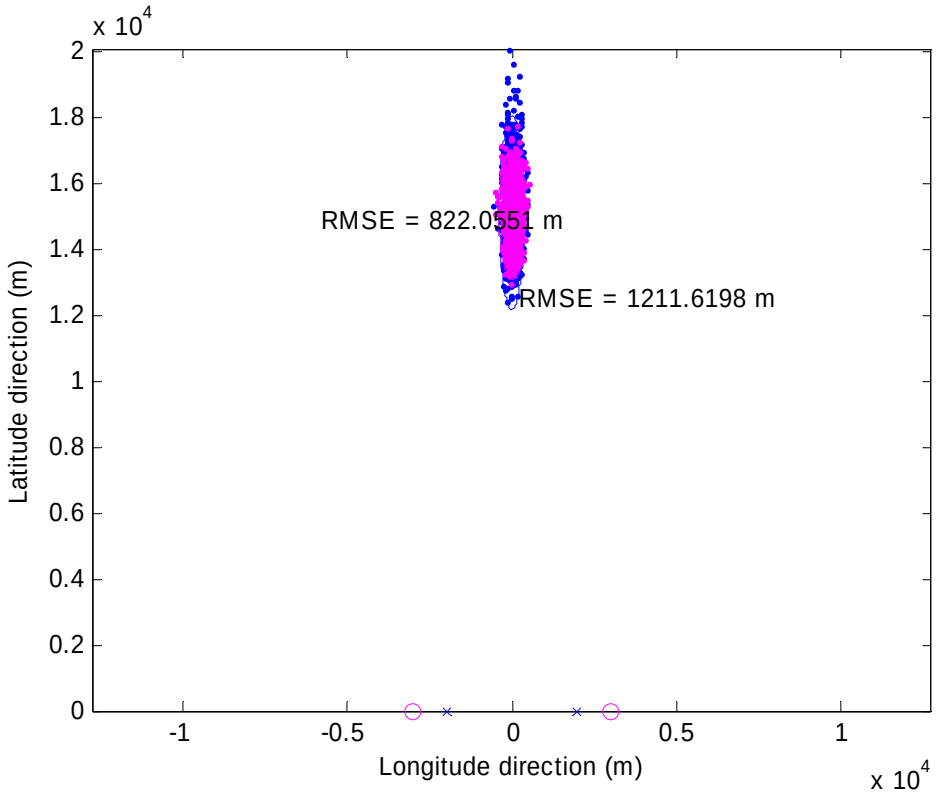

Figure 9: Comparison of emitter location estimates for two receiver pair separations. The emitter is at 15 km from the midpoint of the line joining the two receiver pairs. The "x" plot symbols mark the two receiver pairs separated by 4 km; the 1000 estimates and the 95% concentration ellipse are in blue. The "o" plot symbols indicate the two receiver pairs separated by 6 km; the corresponding 1000 estimates and the 95% concentration ellipse are in magenta.

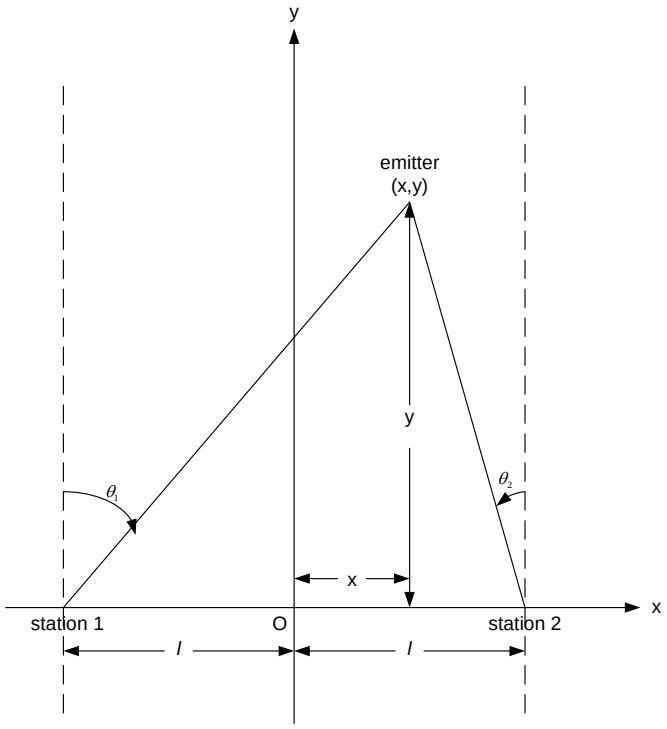

Figure 10: Two-dimensional emitter geolocation based on bearings measured by two stations.

where $\varepsilon_1, \varepsilon_2$ are the range measurement errors of the receivers at station 1; $\varepsilon_3, \varepsilon_4$ those of the receivers at station 2; and 2*a* is the separation between receivers at each station. The ε_i's are assumed to be statistically independent Gaussian random variables, of zero mean and variance σ^2. The bearing errors are therefore independent, zero-mean Gaussian random variables with variances

$$\overline{(\delta\theta_1)^2} = \frac{\sigma^2}{2a^2\cos^2\theta_1}, \qquad \overline{(\delta\theta_2)^2} = \frac{\sigma^2}{2a^2\cos^2\theta_2}. \tag{35}$$

Calculating the partial derivatives in Eq. (33) and making use of Eq. (35), we find that

$$\overline{(\delta x)^2} = \frac{2l^2\sigma^2}{a^2\sin^4(\theta_1-\theta_2)}\left(\frac{\sin^2\theta_2\cos^2\theta_2}{\cos^2\theta_1} + \frac{\sin^2\theta_1\cos^2\theta_1}{\cos^2\theta_2}\right), \tag{36}$$

$$\overline{(\delta y)^2} = \frac{2l^2\sigma^2}{a^2\sin^4(\theta_1-\theta_2)}\left(\frac{\cos^4\theta_2}{\cos^2\theta_1} + \frac{\cos^4\theta_1}{\cos^2\theta_2}\right), \tag{37}$$

$$\overline{\delta x \delta y} = \frac{2l^2\sigma^2}{a^2 \sin^4(\theta_1 - \theta_2)} \left(\frac{\sin\theta_2 \cos^3\theta_2}{\cos^2\theta_1} + \frac{\sin\theta_1 \cos^3\theta_1}{\cos^2\theta_2} \right). \tag{38}$$

The RMS error, ε_r, is, from Eqs. (36) and (37),

$$\begin{aligned} \varepsilon_r &= \sqrt{\overline{(\delta x)^2} + \overline{(\delta y)^2}} \\ &= \frac{\sqrt{2} l\sigma}{a \sin^2(\theta_1 - \theta_2)} \sqrt{\frac{\cos^2\theta_2}{\cos^2\theta_1} + \frac{\cos^2\theta_1}{\cos^2\theta_2}} \,. \end{aligned} \tag{39}$$

For the special case where the emitter is on the *y*-axis, $\theta_2 = -\theta_1$, and the RMS error reduces to

$$\varepsilon_r = \frac{2l\sigma}{a \sin^2 2\theta_1} = \left(\frac{l\sigma}{2a} \right) \frac{\left[1 + (l/y)^2 \right]^2}{(l/y)^2}, \tag{40}$$

where the second equality follows by expressing θ_1 in terms of *l* and the emitter *y*-coordinate, *y*. This special position of the emitter coincides with the geometry considered in Figures 8 and 9. In Table 1, we compare the RMS error as calculated from Eq. (40) with that obtained from simulation for the three combinations of separation between receiver pairs and emitter range. It seems that the simple model considered here gives quite a good description of the RMS error. It may be useful for establishing a lower bound for the RMS error incurred in a three-dimensional, curved-Earth location of an emitter.

Table 1: Comparison of RMS errors calculated from Eq. (40) with $2a = 10$ *m,* $\sigma = 0.1$ *m with those from Monte Carlo simulations.*

l, half the separation between receiver pairs (km)	*y*, emitter range from midpoint of pair separation (km)	RMS error (m)	
		From Eq. (40)	From simulation
2	10	540.8	548.2
2	15	1165.4	1211.6
3	15	811.2	822.1

To study the dependence of the RMS error on an arbitrary emitter position, we set up a 10 km × 10 km grid in the first quadrant, with a grid spacing of 10 m in both horizontal and vertical directions. The emitter is placed at each grid point in turn and the corresponding RMS error is calculated from Eq. (39). Points on the *x*-axis are excluded since the RMS error is infinite at these points due to emitter position ambiguity. Contours of constant RMS error are then produced, five of which are shown in Figure 11. The level values are the RMS errors in metres. Due to the symmetric placement of the receiver pairs, one of which is shown marked by "x" on the *x*-axis, only contours in the first quadrant need to be generated. As might be expected, the emitter position estimator performs best for emitters located in the neighbourhood of the

perpendicular bisector of the line joining the receiver pairs. As an emitter becomes farther removed from this bisector, the same RMS error occurs at a shorter range.

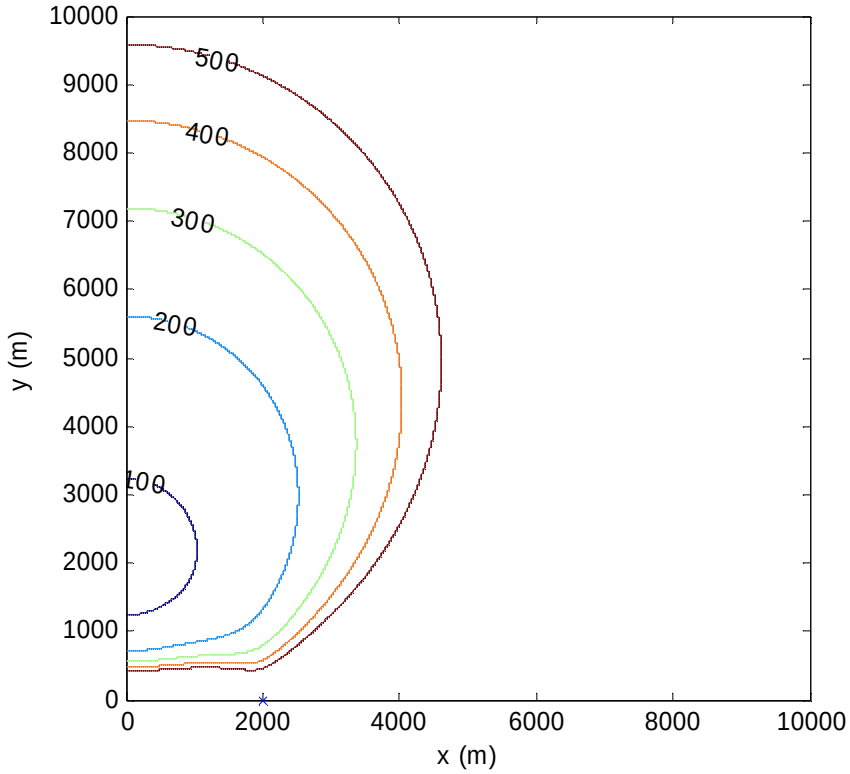

Figure 11: Constant RMS error contours for two-dimensional emitter geolocation based on bearings from two receiver pairs, where each bearing is obtained by measuring the range difference of the emitter from the two receivers of the pair. The receiver pairs, located on the x-axis, are indicated by the "x" plot symbols and are separated by 4 km. Due to symmetry, only contours in the first quadrant are shown. The separation between the receivers of each pair is 10 m, and the range measurement error standard deviation is 0.1 m.

4 Receiver Array on a Single Platform

For this arrangement of receivers, the emitter position is estimated by two methods: one that expresses the position by a closed-form expression and a linearized maximum likelihood estimator. The closed-form expression is derived in Section 4.1. Monte Carlo simulation results for estimation using this method are given in Section 4.2. The LML expression is given in Section 4.3, and the corresponding simulation results are presented in Section 4.4. A plot of the contours of constant RMS error for LML estimation in two dimensions is also shown.

4.1 Closed-Form Method

Let $\mathbf{x}_i, i = 1, \ldots, N$, denote the position of the receivers, $R_i \equiv \|\mathbf{x}_i\|$ the range of receiver *i* from the coordinate system origin, $\mathbf{x}_e$ the position of the emitter, $R_e \equiv \|\mathbf{x}_e\|$ the range of the emitter from the coordinate system origin, D_i the range between receiver *i* and the emitter, and $d_{ij} \equiv D_i - D_j$ the difference between the ranges of receivers *i* and *j* from the emitter. Figure 12 shows receivers 1 and *i*, the emitter, and the defined quantities. It is clear that

$$D_i^2 = (\mathbf{x}_e - \mathbf{x}_i)^T (\mathbf{x}_e - \mathbf{x}_i) = R_e^2 - 2\mathbf{x}_i^T \mathbf{x}_e + R_i^2, \qquad i = 1, \ldots, N. \tag{41}$$

Expressing D_i on the left hand side of Eq. (41) as $d_{i1} + D_1$, we obtain

$$d_{i1}^2 + 2d_{i1}D_1 + D_1^2 = R_e^2 - 2\mathbf{x}_i^T \mathbf{x}_e + R_i^2, \qquad i = 1, \ldots, N. \tag{42}$$

This equation is nonlinear in R_e and D_1, quantities related to the $\mathbf{x}_e$ to be estimated. Equation (42) can be made linear in $\mathbf{x}_e$ and D_1 by subtracting

$$D_1^2 = R_e^2 - 2\mathbf{x}_1^T \mathbf{x}_e + R_1^2$$

from Eq. (42). After some rearrangement of terms, we obtain

$$\frac{R_i^2 - R_1^2 - d_{i1}^2}{2} - d_{i1}D_1 - (\mathbf{x}_i - \mathbf{x}_1)^T \mathbf{x}_e = 0, \qquad i = 2, \ldots, N. \tag{43}$$

Equation (43) is valid for exact range differences d_{i1}. For measured RDs, denoted by $\tilde{d}_{i1}$ and modelled as

$$\tilde{d}_{i1} = d_{i1} + v_{i1}, \tag{44}$$

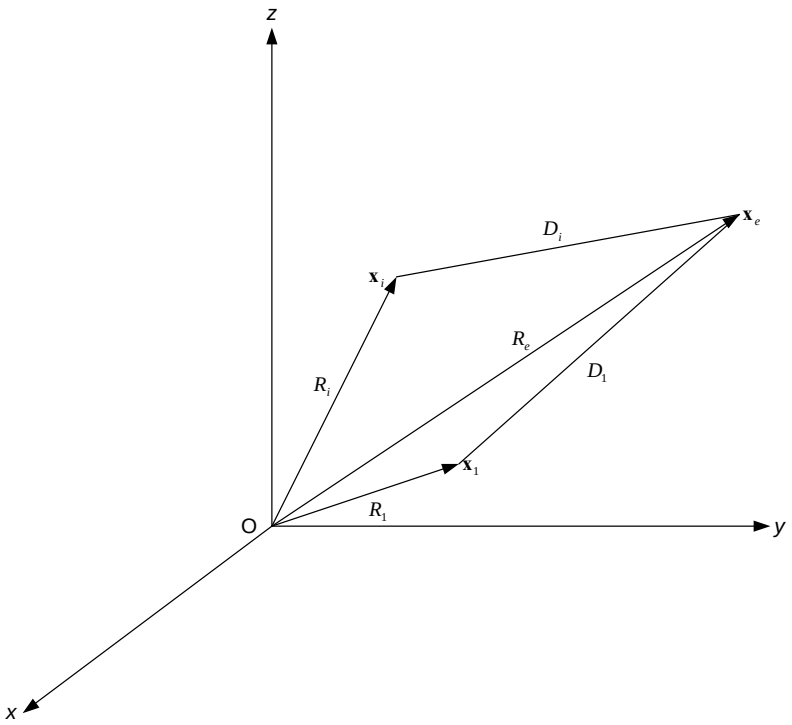

Figure 12: Receiver 1, receiver i *and the emitter, showing the defined quantities.*

where v_{i1} is a zero-mean Gaussian random variable, we find, after substituting Eq. (44) for d_{i1} in the left hand side of Eq. (43) and neglecting the v_{i1}^2 term in the expansion of $\tilde{d}_{i1}^2$, that the measured RDs satisfy

$$\frac{R_i^2 - R_1^2 - \tilde{d}_{i1}^2}{2} - \tilde{d}_{i1} D_1 - (\mathbf{x}_i - \mathbf{x}_1)^T \mathbf{x}_e = -D_i v_{i1}, \qquad i = 2, \ldots, N. \tag{45}$$

This set of $(N-1)$ equations can be written in matrix form as

$$\tilde{\boldsymbol{\delta}} - D_1 \tilde{\mathbf{d}} - \mathbf{S}\mathbf{x}_e = -\mathbf{D}\mathbf{v}, \tag{46}$$

where

$$\tilde{\boldsymbol{\delta}} = \begin{pmatrix} \dfrac{R_2^2 - R_1^2 - \tilde{d}_{21}^{\,2}}{2} \\ \dfrac{R_3^2 - R_1^2 - \tilde{d}_{31}^{\,2}}{2} \\ \vdots \\ \dfrac{R_N^2 - R_1^2 - \tilde{d}_{N1}^{\,2}}{2} \end{pmatrix}, \quad \tilde{\mathbf{d}} = \begin{pmatrix} \tilde{d}_{21} \\ \tilde{d}_{31} \\ \vdots \\ \tilde{d}_{N1} \end{pmatrix}, \quad \mathbf{S} = \begin{pmatrix} (\mathbf{x}_2 - \mathbf{x}_1)^T \\ (\mathbf{x}_3 - \mathbf{x}_1)^T \\ \vdots \\ (\mathbf{x}_N - \mathbf{x}_1)^T \end{pmatrix},$$

$$\mathbf{D} = \begin{pmatrix} D_2 & 0 & \cdots & 0 \\ 0 & D_3 & \cdots & 0 \\ \vdots & \vdots & \ddots & \vdots \\ 0 & 0 & \cdots & D_N \end{pmatrix}, \quad \mathbf{v} = \begin{pmatrix} v_{21} \\ v_{31} \\ \vdots \\ v_{N1} \end{pmatrix}. \tag{47}$$

On the right hand side of Eq. (46), **Dv** is a zero-mean Gaussian random vector with covariance matrix, **R**, given by

$$\mathbf{R} = \mathbf{DQD}, \tag{48}$$

where **Q** is the covariance matrix of **v**:

$$\mathbf{Q} = \overline{\mathbf{v}\mathbf{v}^T}. \tag{49}$$

As noted in Section 3.2, if ε_i is the error associated with the measurement of the separation D_i, then

$$v_{i1} = \varepsilon_i - \varepsilon_1. \tag{50}$$

Therefore, **Q** becomes

$$\mathbf{Q} = \sigma^2 \begin{pmatrix} 2 & 1 & \cdots & 1 \\ 1 & 2 & \cdots & 1 \\ \vdots & \vdots & \ddots & \vdots \\ 1 & 1 & \cdots & 2 \end{pmatrix}. \tag{51}$$

The emitter position is estimated by minimizing the quantity

$$(\tilde{\boldsymbol{\delta}} - D_1\tilde{\mathbf{d}} - \mathbf{S}\mathbf{x}_e)^T \mathbf{R}^{-1} (\tilde{\boldsymbol{\delta}} - D_1\tilde{\mathbf{d}} - \mathbf{S}\mathbf{x}_e), \tag{52}$$

which yields a maximum likelihood estimate. This minimization problem is complicated by the fact that D_1 depends on $\mathbf{x}_e$. To proceed further, we follow the approach of [1] by first regarding D_1 as *given*, obtain the estimate $\hat{\mathbf{x}}_e$ of $\mathbf{x}_e$ in terms of D_1, substitute $\hat{\mathbf{x}}_e$ for $\mathbf{x}_e$ on the left hand

side of Eq. (46), obtain a maximum likelihood estimate for D_1, and substitute this estimate into $\hat{\mathbf{x}}_e$ to obtain the final expression for $\hat{\mathbf{x}}_e$. This series of steps is carried out next.

The minimization of Eq. (52) yields

$$\hat{\mathbf{x}}_e = (\mathbf{S}^T \mathbf{R}^{-1} \mathbf{S})^{-1} \mathbf{S}^T \mathbf{R}^{-1} (\tilde{\boldsymbol{\delta}} - D_1 \tilde{\mathbf{d}}) . \tag{53}$$

Substitution of Eq. (53) for $\mathbf{x}_e$ in Eq. (46) results in

$$\mathbf{P}^{\perp} (\tilde{\boldsymbol{\delta}} - D_1 \tilde{\mathbf{d}}) = -\mathbf{D}\mathbf{v} , \tag{54}$$

where

$$\mathbf{P}^{\perp} = \mathbf{I}_{N-1} - \mathbf{P}, \tag{55}$$

$$\mathbf{P} = \mathbf{S}(\mathbf{S}^T \mathbf{R}^{-1} \mathbf{S})^{-1} \mathbf{S}^T \mathbf{R}^{-1} , \tag{56}$$

and $\mathbf{I}_{N-1}$ in Eq. (55) is the identity matrix of order $(N-1)$. Since Eq. (54) is linear in D_1, a closed-form, maximum likelihood estimate of D_1 can be obtained by minimizing

$$(\tilde{\boldsymbol{\delta}} - D_1 \tilde{\mathbf{d}})^T (\mathbf{P}^{\perp})^T \mathbf{R}^{-1} \mathbf{P}^{\perp} (\tilde{\boldsymbol{\delta}} - D_1 \tilde{\mathbf{d}}) .$$

The solution is

$$\hat{D}_1 = \frac{\tilde{\mathbf{d}}^T (\mathbf{P}^{\perp})^T \mathbf{R}^{-1} \mathbf{P}^{\perp} \tilde{\boldsymbol{\delta}}}{\tilde{\mathbf{d}}^T (\mathbf{P}^{\perp})^T \mathbf{R}^{-1} \mathbf{P}^{\perp} \tilde{\mathbf{d}}} . \tag{57}$$

Substitution of $\hat{D}_1$ for D_1 in Eq. (53) then gives the final closed-form expression for $\hat{\mathbf{x}}_e$:

$$\hat{\mathbf{x}}_e = (\mathbf{S}^T \mathbf{R}^{-1} \mathbf{S})^{-1} \mathbf{S}^T \mathbf{R}^{-1} \left[\mathbf{I}_{N-1} - \frac{\tilde{\mathbf{d}} \tilde{\mathbf{d}}^T (\mathbf{P}^{\perp})^T \mathbf{R}^{-1} \mathbf{P}^{\perp}}{\tilde{\mathbf{d}}^T (\mathbf{P}^{\perp})^T \mathbf{R}^{-1} \mathbf{P}^{\perp} \tilde{\mathbf{d}}} \right] \tilde{\boldsymbol{\delta}} . \tag{58}$$

Equation (58) allows the emitter position to be estimated given a set of receiver positions, a set of measured RDs, and the covariance matrix **R**. From Eq. (48), it is seen that **R** depends on the receiver-emitter separations $D_2, \ldots, D_N$, which are unknown. As a first approximation, we assume that the emitter is far from the receivers, so that $D_2, \ldots, D_N$ are approximately the emitter range R_e. In this approximation, $\mathbf{R} \approx R_e^2 \mathbf{Q}$. From Eq. (56), it is seen that **P** is independent of R_e, which is cancelled out. Therefore, $\mathbf{P}^{\perp}$ is independent of R_e. The same cancellation of R_e occurs in Eq. (58). Therefore, knowledge of R_e is not needed to obtain the first approximation to $\hat{\mathbf{x}}_e$. Once this approximation is obtained, we can compute the separations between the receivers and the emitter and thus obtain a more accurate **R**. The calculation of **P**, $\mathbf{P}^{\perp}$, and $\hat{\mathbf{x}}_e$ is repeated

based on this more accurate **R**, and so on. It is found from the simulations below that it is not necessary to repeat this procedure more than twice.

4.2 Closed-Form Method Simulation Results

Monte Carlo simulations are carried out to evaluate the accuracy of the closed-form method for the two receiver configurations shown in Figure 13. For the five-receiver array, adjacent-receiver separations of 10 m and 20 m are considered. For the nine-receiver array, only 20 m separation is used.

We first note that if the number of receivers is four, **S** is a 3×3 matrix, **P** in Eq. (56) reduces to an identity matrix, $\mathbf{P}^{\perp}$ becomes a zero matrix, and the above method fails. Therefore, a minimum of five receivers is required if the above method is to be used for emitter position estimation. The receivers should not be coplanar, since then for a given set of RDs, the emitter can be on either side of the receiver plane. This is reflected in the matrix $\mathbf{S}^T\mathbf{R}^{-1}\mathbf{S}$ being singular and therefore the emitter position cannot be estimated.

A simulation run involves the following processing. A position is chosen for the emitter, for example, $(1000,1000,0)^T$ metres. The *N* exact separations between the receivers and the emitter are calculated. A set of *N* zero-mean, Gaussian-distributed random numbers with standard deviation σ is generated and added to the exact receiver-emitter separations. The separation of receiver 1 from the emitter is subtracted from the other receiver-emitter separations to simulate a set of $(N-1)$ measured RDs, $\tilde{d}_{i1}, i=2,\ldots,N$. The vectors $\tilde{\boldsymbol{\delta}}$ and $\tilde{\mathbf{d}}$ are then obtained from Eq. (47), the matrix **P** from Eq. (56), $\mathbf{P}^{\perp}$ from Eq. (55), and the emitter position estimate $\hat{\mathbf{x}}_e$ from Eq. (58). The treatment of the matrix **R** is as described at the end of Section 4.1. It is seen from Eq. (58) that because of the cancellation of σ^2 in $\mathbf{R}^{-1}$, $\hat{\mathbf{x}}_e$ does not depend on σ explicitly; its dependence on σ is through $\tilde{\boldsymbol{\delta}}$ and $\tilde{\mathbf{d}}$.

The emitter position is estimated 10,000 times in a simulation run. At the end of a run, estimation statistics are obtained, as described in Section 3.2. These include the mean estimate $\overline{\hat{\mathbf{x}}_e}$, the covariance matrix **C**, the bias **b**, and the RMS error ε_r. The top panels and the bottom left panel of Figure 14 show the emitter position estimates for three values of σ: 0.1 m, 0.01 m and 0.001 m. The receiver array is the five-element array of Figure 13(a), with 10 m spacing between adjacent receivers. Since the *z*-direction estimates are negligible compared with the *x*- and *y*-direction estimates, only the projections of the estimates on the *xy*-plane are shown. Each of the top panels shows approximately 1,000 estimates (approximately because of the cropping of the full display to smaller *x* and *y* ranges). The green "+" symbol represents the receiver array and the red "x" marks the exact emitter position of $(1000,1000,0)^T$ m. For $\sigma = 0.1$ m, there are as many estimates in the wrong third quadrant as there are in the correct first quadrant. This situation improves as σ is reduced. However, for both $\sigma = 0.1$ m and $\sigma = 0.01$ m, the mean estimate varies from one simulation run to another. Only for $\sigma = 0.001$ m is there stabilization in the mean estimate.

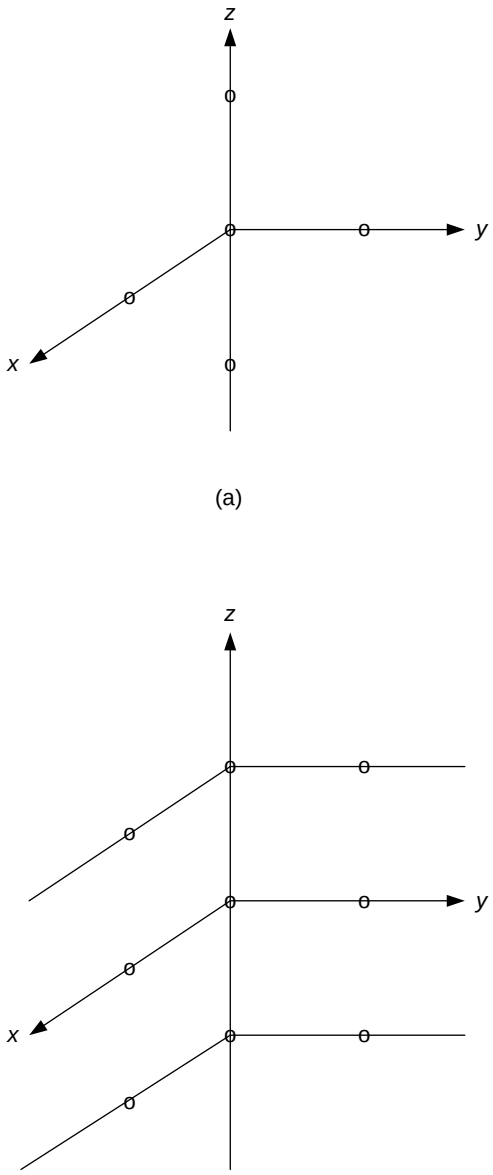

Figure 13: A five-receiver array (a) and a nine-receiver array (b) considered in the simulations. Adjacent-receiver spacing of 10 m and 20 m are considered for array (a) and spacing of 20 m is used for array (b).

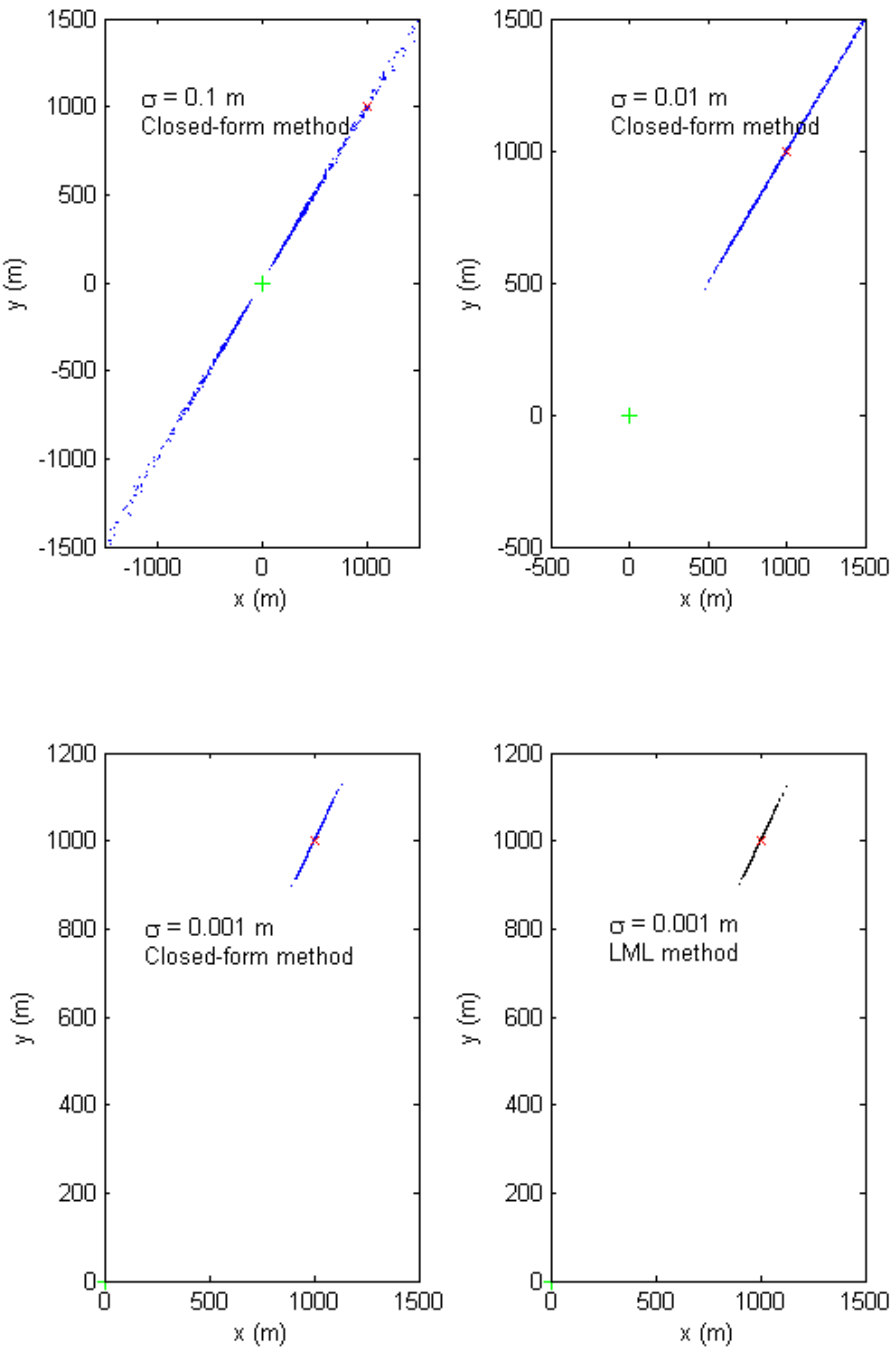

Figure 14: Emitter position estimates on the xy*-plane for the five-receiver array of Figure 11(a), with adjacent-receiver spacing of 10 m, and with emitter at* $(1000,1000,0)^T$ *m. The top left, top right and bottom left panels show estimates from the closed-form method for* $\sigma = 0.1$ *m,* $\sigma = 0.01$ *m and* $\sigma = 0.001$ *m, respectively. The bottom right panel shows the estimates from the LML method for* $\sigma = 0.001$ *m.*

Table 2: Simulation statistics from the closed-form method for five combinations of receiver configuration and emitter position. Each run is made with $\sigma = 0.001$ m and consists of 10,000 Monte Carlo trials.

Array config.	Adjacent Rx spacing (m)	Exact emitter position (m)	*x* mean est. (m)	*x* std. dev. (m)	RMS error (m)
5-Rx	10	(1000, 1000, 0)	1001.4	34.8	49.3
5-Rx	20	(1000, 1000, 0)	1000.1	8.6	12.2
5-Rx	20	(5000, 5000, 0)	5007.4	218.7	309.5
9-Rx	20	(5000, 5000, 0)	4989.0	123.4	175.2
9-Rx	20	(10000, 10000, 0)	9919.3	492.0	705.1

The *x* component of the mean estimate, the *x*-component standard deviation and the RMS error are shown in Table 2 for five combinations of receiver configuration and emitter position. Due to the symmetry of the receiver array and the emitter position, the *x* and *y* components of the mean estimate are equal, and the *z* component is negligibly small. Therefore, only the *x* component of the mean estimate is included in the table. Similarly, the *x*- and *y*-component standard deviations are equal, and the *z* component is negligible. (The estimate standard deviations are the square roots of the diagonal elements of **C**.) Therefore, only the *x*-component standard deviation is shown. All runs are made with $\sigma = 0.001$ m and 10,000 trials. As one would expect, as the receiver separation and/or number of receivers increases, the estimator performance improves, and as the emitter range increases, the performance worsens.

From the last row of the table, it is seen that in order to be able to locate an emitter at a useful range of the order of 15 km with a RMS error of about 700 m, ranges would have to be measured to an accuracy of about 1 mm and the receiver array should have about 10 receivers with adjacent spacing of 20 m. The required range measurement accuracy is 100 times the current capability of about 10 cm. The placement of such a physically large array on a ship where space is limited is likely to be a problem. The large number of receivers required may also exceed cost constraints.

4.3 Linearized Maximum Likelihood Method

We begin with Eq. (44) for the measured RD $\tilde{d}_{i1}$:

$$\tilde{d}_{i1} = d_{i1} + v_{i1} = D_i - D_1 + v_{i1}. \tag{59}$$

In terms of the emitter rectangular coordinates *x*, *y*, *z* (i.e., $(x\ y\ z)^T = \mathbf{x}_e$) and receiver *i* rectangular coordinates x_i, y_i, z_i (i.e., $(x_i\ y_i\ z_i)^T = \mathbf{x}_i$), D_i is given by

$$D_i = \sqrt{(x - x_i)^2 + (y - y_i)^2 + (z - z_i)^2}$$

and its partial derivatives are given by

$$\frac{\partial D_i}{\partial x} = \frac{(x - x_i)}{D_i}, \quad \frac{\partial D_i}{\partial y} = \frac{(y - y_i)}{D_i}, \quad \frac{\partial D_i}{\partial z} = \frac{(z - z_i)}{D_i}.$$

The right hand sides of these partial derivatives are the components of the unit vector, $\mathbf{u}_i$, from receiver *i* to the emitter. The expansion of D_i in a Taylor series about $\mathbf{x}_e = \mathbf{x}_0$ is, to first order,

$$D_i \approx D_{i0} + \mathbf{u}_{i0}^T(\mathbf{x}_e - \mathbf{x}_0), \quad i = 1, \ldots, N,$$

where D_{i0} and $\mathbf{u}_{i0}$ are D_i and $\mathbf{u}_i$ evaluated at $\mathbf{x}_e = \mathbf{x}_0$. Therefore, Eq. (59) becomes

$$\tilde{d}_{i1} \approx d_{i1,0} + (\mathbf{u}_{i0} - \mathbf{u}_{10})^T(\mathbf{x}_e - \mathbf{x}_0) + v_{i1}, \quad i = 2, \ldots, N, \tag{60}$$

where $d_{i1,0} \equiv D_{i0} - D_{10}$. Writing the equations (60) in matrix form, we have

$$\tilde{\mathbf{d}} \approx \mathbf{d}_0 + \mathbf{H}_0(\mathbf{x}_e - \mathbf{x}_0) + \mathbf{v},$$

where

$$\mathbf{d}_0 = \begin{pmatrix} d_{21,0} \\ d_{31,0} \\ \vdots \\ d_{N1,0} \end{pmatrix}, \quad \mathbf{H}_0 = \begin{pmatrix} (\mathbf{u}_{20} - \mathbf{u}_{10})^T \\ (\mathbf{u}_{30} - \mathbf{u}_{10})^T \\ \vdots \\ (\mathbf{u}_{N0} - \mathbf{u}_{10})^T \end{pmatrix}, \tag{61}$$

and $\tilde{\mathbf{d}}$ and $\mathbf{v}$ are as defined in Eq. (47). In view of the fact that $\mathbf{v}$ is a zero-mean, Gaussian random vector with covariance matrix $\mathbf{Q}$, the maximum-likelihood estimate of $\mathbf{x}_e$, $\hat{\mathbf{x}}_e$, can be obtained by minimizing

$$(\tilde{\mathbf{d}} - \mathbf{d}_0 + \mathbf{H}_0\mathbf{x}_0 - \mathbf{H}_0\mathbf{x}_e)^T\mathbf{Q}^{-1}(\tilde{\mathbf{d}} - \mathbf{d}_0 + \mathbf{H}_0\mathbf{x}_0 - \mathbf{H}_0\mathbf{x}_e).$$

The solution is

$$\hat{\mathbf{x}}_e = \mathbf{x}_0 + (\mathbf{H}_0^T\mathbf{Q}^{-1}\mathbf{H}_0)^{-1}\mathbf{H}_0^T\mathbf{Q}^{-1}(\tilde{\mathbf{d}} - \mathbf{d}_0). \tag{62}$$

To obtain an estimate of the emitter position, we choose an initial estimate $\mathbf{x}_0$. The unit vectors $\mathbf{u}_{i0}$ and ranges D_{i0} are calculated, from which $\mathbf{H}_0$ and $\mathbf{d}_0$ can be obtained. The right hand side of Eq. (62) is then evaluated to give the first-iteration estimate. This process is repeated, using the first-iteration estimate as $\mathbf{x}_0$ to obtain the second-iteration estimate, and so on. If this procedure converges, convergence is achieved in five or six iterations. The drawback of this

method is that the initial estimate may not lead to convergence or leads to convergence to a local rather than the absolute minimum.

In our study, the LML method is used mainly as a check of the simulation results obtained with the closed-form method, rather than as a serious contender as an emitter position estimator. Thus in the simulation results of the next section, the initial estimate is set to the best possible choice of actual emitter position.

4.4 Linearized Maximum Likelihood Simulation Results

Table 3: Comparison of simulation statistics from the closed-form and LML methods for the five combinations of receiver configuration and emitter position of Table 2.

Table 1 row no.	Closed-form method			LML method		
	x mean est. (m)	*x* std. dev. (m)	RMS error (m)	*x* mean est. (m)	*x* std. dev. (m)	RMS error (m)
1	1001.4	34.8	49.3	1000.9	34.1	48.2
2	1000.1	8.6	12.2	1000.1	8.5	12.0
3	5007.4	218.7	309.5	5007.2	213.4	301.9
4	4989.0	123.4	175.2	5002.1	112.2	158.7
5	9919.3	492.0	705.1	10008.8	452.5	640.0

Simulations for the five combinations of receiver configuration and emitter position considered in Table 2 are carried out using the LML method. All runs are made with $\sigma = 0.001$ m and 10,000 trials per run. (A run with $\sigma = 0.01$ m fails to converge.) The bottom right panel of Figure 14 shows the first 1,000 estimates for the five-receiver array with adjacent receiver spacing of 10 m and with the emitter at $(1000, 1000, 0)^T$ m. The comparison with the closed-form results with regard to the *x*-component of the mean estimate, the *x*-component standard deviation and the RMS error is shown in Table 3. With the ideal choice of the initial estimate, the LML method yields smaller bias and smaller standard deviation, resulting in a smaller RMS error. However, since such an ideal choice cannot, in general, be made, the drawback of LML makes the closed-form method seem like an attractive alternative.

To study the effect of emitter position on estimator performance, we generate contours of constant RMS error. In the LML method, the position estimate covariance matrix is given by [4]

$$(\mathbf{H}_0^T \mathbf{Q}^{-1} \mathbf{H}_0)^{-1}. \tag{63}$$

Assuming that the bias is negligible, the RMS error can be calculated as the square root of the trace of this matrix. We note that (63) is proportional to σ^2, and therefore the RMS error is proportional to σ. To reduce the amount of computations, we consider the receivers and the emitter to be on a plane. In Figure 15, the three "x" plot symbols at the origin mark the positions of the receivers used in the calculations. These receivers are just the ones on the *xy*-plane of the

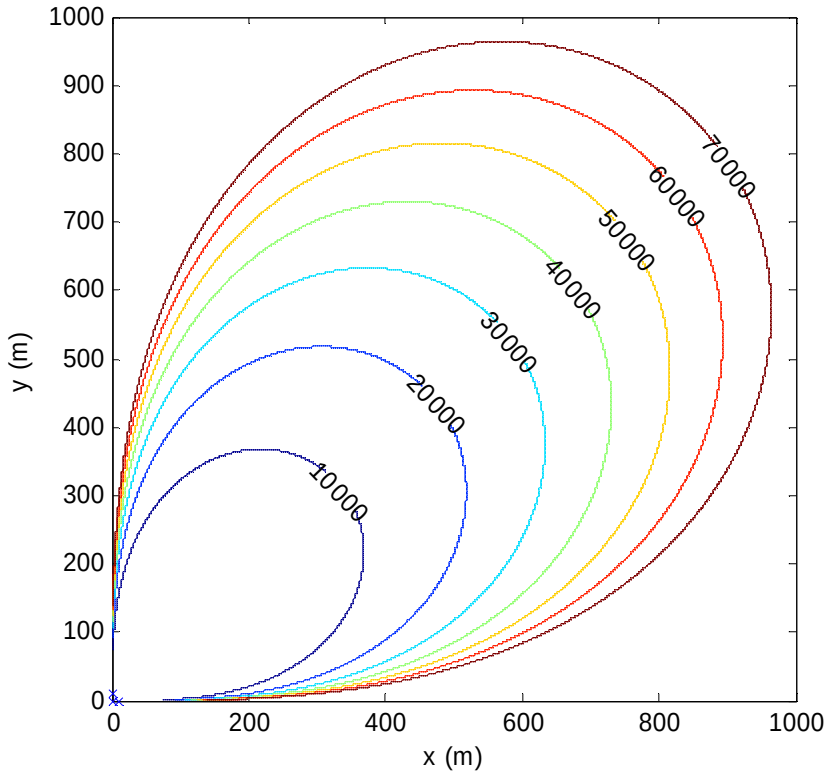

Figure 15: Contours of constant ratio of RMS error to range measurement error standard deviation for two-dimensional emitter geolocation by the LML method. The three receivers are marked by the "x" plot symbols at the origin. The spacing between adjacent receivers is 10 m.

arrays in Figure 13. The adjacent receiver spacing is 10 m. The grid used is $1{,}000 \times 1{,}000$, over an area of 1 km × 1 km. Points on the *x* and *y* axes are excluded, since the estimate covariance matrix does not exist at these points due to emitter position ambiguity. The RMS error is calculated at each grid point and then the contours produced. Figure 15 shows seven such contours. The contour level values are the RMS errors in units of σ. Thus if $\sigma = 0.001$ m, the 70,000 contour corresponds to a RMS error of 70 m. From the first row of Table 3, which is for the five-receiver array of Figure 13(a) with adjacent spacing of 10 m and for an emitter at $(1{,}000, 1{,}000, 0)^T$ m, the LML method RMS error is 48.2 m. Thus the 70 m value is not unreasonable; we expect the RMS error to be larger because of the smaller number of receivers. The estimator performs best for an emitter on the 45° line, where its *x* and *y* coordinates are equal. We expect this to be the case from the symmetry of the receiver-emitter geometry. For an emitter not on this line, it has to be at a closer range for the RMS error to remain the same, or if its range is maintained to be the same, then the RMS error increases.

5 Summary

A method is developed for tracing out, on essentially the Earth's surface, a curve such that the difference in the ranges of each point on the curve from two arbitrarily oriented receivers is a specified amount. The intersection of two such constant RD curves resulting from measured RDs by two pairs of receivers on geographically separated platforms is used to geolocate an emitter that is constrained to move on the Earth's surface. Monte Carlo simulations are carried out to determine the estimation accuracy of this method. For receiver pairs with 10 m baseline, range measurement accuracy of 0.1 m, pair separation of 6 km, and emitter range of 15 km from the midpoint of the line joining the pairs, the RMS error is 820 m. For comparison, geolocation of an emitter at a comparable range with comparable accuracy by a single receiver array would require the array to have nine receivers, adjacent receiver spacing of 20 m, and a much more stringent range measurement accuracy of 1 mm by the receivers. The first approach is therefore the more practical at present. For both geographically-separated pairs and single arrays, the location estimation is highest when there is symmetry in the receiver-emitter geometry, such as the emitter being on the perpendicular bisector of the line joining a pair.

Two-dimensional geolocation by triangulation by two stations is considered as a simple model for location estimation by the intersection of constant RD curves. The expressions derived for the position estimate and its covariance matrix elements are in terms of the baseline and the range measurement accuracy of the receivers of the pairs that constitute the stations. Direct comparison of the RMS error from the model can therefore be made with that from simulations. The model RMS error seems to provide a lower bound.

References

[1] J. O. Smith and J. S. Abel, “Closed-Form Least-Squares Source Location Estimation from Range-Difference Measurements,” IEEE Trans. Acoust., Speech, Signal Processing, vol. 35, no. 12, pp. 1661-1669, December 1987.

[2] Y. T. Chan and K. C. Ho, “A Simple and Efficient Estimator for Hyperbolic Location,” IEEE Trans. Signal Processing, vol. 42, no. 8, pp. 1905-1915, August 1994.

[3] J. M. Delosme, M. Morf and B. Friedlander, “Source Location from Time Differences of Arrival: Identifiability and Estimation,” Proc. IEEE Int. Conf. Acoust., Speech, Signal Processing, 1980, pp. 818-824.

[4] D. J. Torrieri, “Statistical Theory of Passive Location Systems,” IEEE Trans. Aerosp. Electron. Syst., vol. 20, no. 2, pp. 183-198, March 1984.

[5] W. H. Foy, “Position-Location Solution by Taylor-Series Estimation,” IEEE Trans. Aerosp. Electron. Syst., vol. 12, no. 2, pp. 187-194, March 1976.

DOCUMENT CONTROL DATA

(Security classification of title, body of abstract and indexing annotation must be entered when the overall document is classified)

1. ORIGINATOR (The name and address of the organization preparing the document. Organizations for whom the document was prepared, e.g. Centre sponsoring a contractor's report, or tasking agency, are entered in section 8.)

Defence R&D Canada – Ottawa
3701 Carling Avenue
Ottawa, Ontario K1A 0Z4

2. SECURITY CLASSIFICATION (Overall security classification of the document including special warning terms if applicable.)

UNCLASSIFIED

3. TITLE (The complete document title as indicated on the title page. Its classification should be indicated by the appropriate abbreviation (S, C or U) in parentheses after the title.)

The determination of constant range-difference curves on a spherical surface and its application to emitter geolocation

4. AUTHORS (last name, followed by initials – ranks, titles, etc. not to be used)

Lee, J. P. Y.; Sung, S. H.

5. DATE OF PUBLICATION (Month and year of publication of document.)

August 2009

6a. NO. OF PAGES (Total containing information, including Annexes, Appendices, etc.)

52

6b. NO. OF REFS (Total cited in document.)

5

7. DESCRIPTIVE NOTES (The category of the document, e.g. technical report, technical note or memorandum. If appropriate, enter the type of report, e.g. interim, progress, summary, annual or final. Give the inclusive dates when a specific reporting period is covered.)

Technical Memorandum

8. SPONSORING ACTIVITY (The name of the department project office or laboratory sponsoring the research and development – include address.)

Defence R&D Canada – Ottawa
3701 Carling Avenue
Ottawa, Ontario K1A 0Z4

9a. PROJECT OR GRANT NO. (If appropriate, the applicable research and development project or grant number under which the document was written. Please specify whether project or grant.)

15df01

9b. CONTRACT NO. (If appropriate, the applicable number under which the document was written.)

10a. ORIGINATOR'S DOCUMENT NUMBER (The official document number by which the document is identified by the originating activity. This number must be unique to this document.)

DRDC Ottawa TM 2009-119

10b. OTHER DOCUMENT NO(s). (Any other numbers which may be assigned this document either by the originator or by the sponsor.)

11. DOCUMENT AVAILABILITY (Any limitations on further dissemination of the document, other than those imposed by security classification.)

Unlimited

12. DOCUMENT ANNOUNCEMENT (Any limitation to the bibliographic announcement of this document. This will normally correspond to the Document Availability (11). However, where further distribution (beyond the audience specified in (11) is possible, a wider announcement audience may be selected.))

13. ABSTRACT (A brief and factual summary of the document. It may also appear elsewhere in the body of the document itself. It is highly desirable that the abstract of classified documents be unclassified. Each paragraph of the abstract shall begin with an indication of the security classification of the information in the paragraph (unless the document itself is unclassified) represented as (S), (C), (R), or (U). It is not necessary to include here abstracts in both official languages unless the text is bilingual.)

This report focuses on the problem of emitter geolocation by measuring the range differences of the emitter from a number of receivers. Two receiver arrangements are considered. In the first arrangement, receiver pairs are located on geographically dispersed platforms. An algorithm is developed that traces out, on essentially the Earth's surface, a curve where each point is at a specified range difference from two receivers. The intersections of such curves, one from the receiver pair on each platform, then yield an estimate of the emitter position. Monte Carlo simulations are carried out to determine the root-mean-square error associated with the intersection point of two such curves. In the second arrangement, several receivers are clustered into an array located on a single platform. Two location estimation methods are employed in Monte Carlo simulations to study the estimation accuracy. In view of the much higher range measurement accuracy required when geolocation is to be performed by a single array, the restriction on the receiver spacing due to space limitations on the platform, and the restriction on the number of receivers due to cost considerations, the first receiver arrangement seems to be the more practical at present.

Le présent rapport porte sur la géolocalisation d'émetteurs au moyen des différences entre les distances de l'émetteur par rapport aux divers récepteurs. Deux configurations de récepteurs sont examinées. Pour la première configuration, des paires de récepteurs ont été placées sur des plates-formes géographiquement dispersées. Un algorithme a été mis au point pour dessiner, essentiellement à la surface de la Terre, une courbe dont chaque point correspond à une différence de distance connue de deux récepteurs. Le point d'intersection de ces courbes, une courbe pour la paire de récepteurs de chaque plate-forme, donne la position estimée de l'émetteur. Des simulations de Monte Carlo ont été effectuées afin de déterminer l'erreur quadratique moyenne liée au point d'intersection de ces deux courbes. Pour la seconde configuration, plusieurs récepteurs ont été groupés dans un réseau situé sur une seule plate-forme. Deux méthodes d'estimation de la position sont utilisées dans les simulations de Monte Carlo afin d'étudier la précision des estimations. Étant donné que les mesures de distance utilisées pour effectuer la géolocalisation à partir d'un seul réseau doivent être très précises, que la distance entre les émetteurs est limitée par l'espace disponible sur la plate-forme et que le nombre de récepteurs est limité pour des raisons de coût, la première configuration de récepteurs semble la plus pratique pour le moment.

14. KEYWORDS, DESCRIPTORS or IDENTIFIERS (Technically meaningful terms or short phrases that characterize a document and could be helpful in cataloguing the document. They should be selected so that no security classification is required. Identifiers, such as equipment model designation, trade name, military project code name, geographic location may also be included. If possible keywords should be selected from a published thesaurus, e.g. Thesaurus of Engineering and Scientific Terms (TEST) and that thesaurus identified. If it is not possible to select indexing terms which are Unclassified, the classification of each should be indicated as with the title.)

constant range-difference curves; intersection of cone with spherical surface; coordinate transformations; rotation matrices; emitter geolocation; range difference measurements; bearing measurements; triangulation; maximum likelihood estimation; Monte Carlo simulations; root-mean-square error contours

Defence R&D Canada

Canada's leader in Defence
and National Security
Science and Technology

R & D pour la défense Canada

Chef de file au Canada en matière
de science et de technologie pour
la défense et la sécurité nationale

www.drdc-rddc.gc.ca